EUROPEAN ORGANIZATION FOR NUCLEAR RESEARCH (CERN)

CERN-EP-2025-217
2025/11/19

CMS-B2G-24-007

Search for heavy Hγ and Zγ resonances with a bottom quark-antiquark pair in the final state in proton-proton collisions at $\sqrt{s} = 13\,\mathrm{TeV}$

The CMS Collaboration*

Abstract

A search for heavy resonances decaying into a Higgs boson (H) or a Z boson and a photon (γ), with the H or Z bosons decaying to a bottom quark-antiquark pair ($\mathrm{b\overline{b}}$) is presented. The analysis is performed using proton-proton collision data at $\sqrt{s} = 13\,\mathrm{TeV}$ collected by the CMS experiment at the CERN Large Hadron Collider, corresponding to an integrated luminosity of $138\,\mathrm{fb}^{-1}$. The analyzed events contain a photon and a massive large-radius jet originating from a Lorentz-boosted $\mathrm{b\overline{b}}$ system. An advanced transformer-based algorithm classifies jets according to their substructure and quark flavors, forming a tagger that identifies jets as candidates from $\mathrm{H/Z \to b\overline{b}}$ decays. A set of parametric functions is used to fit the photon-jet invariant mass spectrum and to extract potential signals. No significant excess is observed above the standard model expectations. The results set upper limits at 95% confidence level on the product of the cross section and the branching fraction for spin-1 Hγ resonances and spin-0 Zγ resonances, below 0.1 and 0.3 fb, respectively, representing the most stringent limits to date.

Submitted to Science Bulletin

*See Appendix A for the list of collaboration members

1 Introduction

Exploring extensions of the standard model (SM) is one of the main objectives of the CERN Large Hadron Collider (LHC) research program. Physics beyond the SM (BSM) may reveal itself through the production of new heavy particles that decay into SM particles. Numerous searches for massive resonances decaying into pairs of SM particles, such as dijet or diboson analyses [1–19], have been carried out with the goal of uncovering any possible hints of BSM physics.

This paper presents a search for resonances that decay into a photon (γ) and either a Higgs boson (H) or a Z boson, with the H or Z boson subsequently decaying into a bottom quark-antiquark pair ($b\overline{b}$). In particular, this analysis considers a narrow-width spin-1 resonance, denoted as Z', decaying as $Z' \to H\gamma \to b\overline{b}\gamma$, as well as a narrow- or broad-width spin-0 resonance, S, decaying as $S \to Z\gamma \to b\overline{b}\gamma$. The analysis focuses on heavy Z' and S resonances that decay into a γ and a Lorentz-boosted $b\overline{b}$ quark system. The hadronization products of the $b\overline{b}$ system form a single, massive, large-radius jet (j) with two subjets, typically featuring displaced secondary vertices, which are characteristic of the hadronization of b quarks.

The Z' resonant signal is predicted by several BSM scenarios, such as the examples studied in Ref. [20]. The one-loop $Z' \to H\gamma$ process discussed in that paper is used as the benchmark signal model in this analysis, as in earlier studies [10, 21]. The Z' resonance is a neutral spin-1 gauge boson associated with an additional U(1)′ symmetry that extends the SM electroweak sector, and because its decay to $H\gamma$ is assumed to proceed through a heavy-quark loop, the corresponding branching fraction is typically 10^{-5} or smaller. Nonetheless, these models predict scenarios in which a significant portion of the parameter space leaves open the possibility that the $Z' \to H\gamma$ mode could be observed, owing to the small SM background. In this analysis, the fractional width of the Z' boson, $\Gamma_{Z'}/m_{Z'}$, where $m_{Z'}$ ($\Gamma_{m_{Z'}}$) is the Z' boson mass (intrinsic width), is assumed to be narrow and the search is conducted for signal masses in the range of 0.7–3.5 TeV.

Neutral massive bosons with spin 0 or 2 can also decay via the $Z\gamma$ channel. Such decays are predicted in various BSM extensions, including technicolor [22] and little Higgs [23] models, as well as models with extended Higgs sectors [24, 25] and extra spatial dimensions [26, 27]. In this analysis, the $Z\gamma$ signal considered is a heavy scalar boson, denoted in this paper as S, similar to the SM Higgs boson. This model has been used as a benchmark in similar analyses, including Refs. [9, 28]. Although the $Z\gamma$ channel results are interpreted for scalar resonances, they are approximately applicable to spin-2 states, as the signal acceptance is only weakly dependent on the resonance's spin [29]. For the $S \to Z\gamma$ process, three width scenarios of Γ_S/m_S are considered, with signal hypotheses in the m_S range 0.7–3.5 TeV.

In both the $Z' \to H\gamma$ and $S \to Z\gamma$ signal scenarios, the H or Z boson can decay hadronically into a $b\overline{b}$ system. The branching fraction $\mathcal{B}(H \to b\overline{b}) \approx 58\%$ is the largest among all Higgs boson decay modes, while the Z boson branching fraction $\mathcal{B}(Z \to b\overline{b}) \approx 15\%$ is also a sizable Z boson decay mode. Since $m_{Z'}, m_S > 0.7$ TeV, the $b\overline{b}$ system typically receives a significant Lorentz boost, and its hadronization products can be reconstructed as a single, large-radius jet. Figure 1 displays schematic diagrams of the signal processes probed.

The analysis employs advanced machine-learning (ML) techniques to select $H \to b\overline{b}$ and $Z \to b\overline{b}$ candidate jets. For the identification of candidate jets based on their reconstructed mass, an ML-based jet mass variable is constructed using the PARTICLENET algorithm [30], which has been shown to improve the jet mass resolution by approximately 20% [31] compared to the previously used soft-drop mass technique [32] for jets formed by the $H \to b\overline{b}$

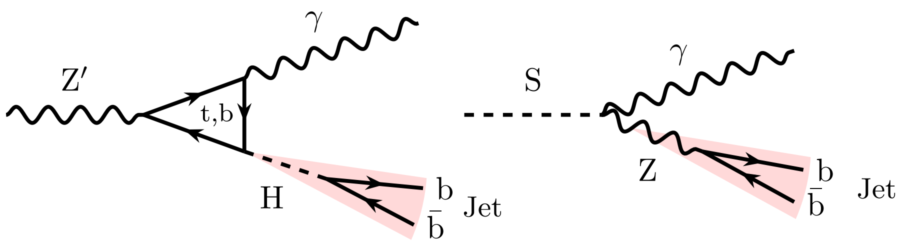

Figure 1: Schematic illustration indicating the topology of the signal processes under consideration in this search. The spin-1 $Z' \to H\gamma \to b\bar{b}\gamma$ signal scenario is shown on the left, and the spin-0 $S \to Z\gamma \to b\bar{b}\gamma$ signal scenario is shown on the right.

decays. The substructure of candidate jets is analyzed using the state-of-the-art global particle transformer (GLOPART) algorithm [33], which provides discriminant variables that efficiently suppress background processes, leading to a significantly improved identification of jets with the $b\bar{b}$ structure.

This analysis uses proton-proton (pp) collision data collected by the CMS experiment at $\sqrt{s} = 13\,\text{TeV}$ in 2016–2018, corresponding to an integrated luminosity of $138\,\text{fb}^{-1}$ [34–36]. The data are divided into four signal regions (SRs) based on the jet mass and the $b\bar{b}$ tagger score. The invariant mass of the γ+jet system ($m_{j\gamma}$) is studied in each SR for the presence of signal, which manifests as a peak in the $m_{j\gamma}$ spectrum on top of a smoothly falling background. While this search is optimized for $H\gamma$ and $Z\gamma$ resonant signals, it is also moderately sensitive to other resonances (X) not specifically targeted by the analysis, including processes involving photon pairs, such as $X \to HA \to b\bar{b}\gamma\gamma$ and $X \to ZA \to b\bar{b}\gamma\gamma$ (with A representing a light hypothetical (pseudo)scalar particle). Indeed, for A masses at the GeV scale or below, the two photons would be collimated and reconstructed as a single photon, yielding the same signature as in this analysis.

This paper is organized as follows. Section 2 describes the CMS detector. The background Monte Carlo (MC) simulated samples and the signal modeling are discussed in Section 3. The triggers employed for data collection and the event reconstruction are described in Section 4. Event selection and categorization are presented in Section 5. Section 6 describes the estimation of the SM background. Systematic uncertainties are presented in Section 7. The results and their interpretation are given in Section 8. The paper is summarized in Section 9. Tabulated results for this analysis are provided in the HEPData record [37].

2 The CMS detector

The CMS apparatus [38, 39] is a multipurpose, nearly hermetic detector, designed to trigger on [40–42] and identify electrons, muons, photons, and (charged and neutral) hadrons [43–45]. Its central feature is a superconducting solenoid of 6 m internal diameter, providing a magnetic field of 3.8 T. Within the solenoid volume are a silicon pixel and a strip tracker, a lead tungstate crystal electromagnetic calorimeter (ECAL), and a brass and scintillator hadron calorimeter (HCAL), each composed of a barrel and two endcap sections. Forward calorimeters extend the pseudorapidity (η) coverage provided by the barrel and endcap detectors. Muons are reconstructed using gas-ionization detectors embedded in the steel flux-return yoke outside the solenoid. More detailed descriptions of the CMS detector, together with a definition of the coordinate system used and the relevant kinematic variables, can be found in Refs. [38, 39].

The ECAL consists of 75 848 $PbWO_4$ crystals, each with a transverse dimension approximately matching the Molière radius of the material and 25 radiation lengths in depth. The ECAL barrel section covers the region $|\eta| < 1.48$, while the two endcap sections extend over $1.48 < |\eta| < 3.00$. In the barrel section, an energy resolution of about 1% is achieved for unconverted or late-converting photons with energies of a few tens of GeV. The energy resolution of the remaining, converted barrel photons is about 1.3% up to $|\eta| = 1$, changing to about 2.5% at $|\eta| = 1.4$. In the endcaps, the energy resolution is about 2.5% for unconverted or late-converting photons, and between 3 and 4% for converted photons [43, 46]. The energy deposits in ECAL and HCAL cells are summed to define the calorimeter tower energies, which are subsequently used to provide the energies and directions of hadronic jets. The silicon tracker measures charged particles within the pseudorapidity range $|\eta| < 3.0$. During the LHC running period when the data used in this Letter were recorded, the silicon tracker consisted of 1856 silicon pixel and 15 148 silicon strip detector modules. Details on the pixel detector can be found in Ref. [47]. For nonisolated particles of transverse momentum (p_{T}) in 1–10 GeV range and $|\eta| < 3.0$, the track resolutions are typically 1.5% in p_{T} and 20–75 μm in the transverse impact parameter [48]

Events of interest are selected using a two-tiered trigger system. The first level, composed of custom hardware processors, uses information from the calorimeters and muon detectors to select events at a rate of around 100 kHz within a fixed latency of 4 μs [40]. The second level, known as the high-level trigger, consists of a farm of processors running a version of the full event reconstruction software optimized for fast processing, and reduces the event rate to a few kHz before data storage [41, 42].

3 Simulated samples and signal modeling

The selection optimization is performed using simulated signal and SM background samples. These include events from quantum chromodynamics (QCD) multijet production, W and Z boson production, and $\mathrm{t\bar{t}}$ production, each accompanied by an additional photon. Additional samples of the same processes without a photon are also considered, accounting for cases where hadrons or electrons may be misidentified as photons. The overlap between processes with and without photons is resolved by applying a generator-level disambiguation procedure. For example, in the QCD process, only events without prompt photons—collectively referred to as nonprompt—are retained, while for the QCD+γ process, only events with a prompt photon are kept. Events for all processes are generated at leading order (LO) or next-to-LO (NLO) precision using the MADGRAPH5_aMC@NLO 2.4.2 generator [49].

For both signal and background samples, fragmentation and hadronization are simulated with PYTHIA 8.230 [50]. The underlying event is modeled using the CP5 tune [51], and GEANT4 [52] is used to simulate the detector response. Additional pp interactions occurring in the same or nearby bunch crossings, known as pileup (PU), are overlaid on the main collision during simulation. The NNPDF 3.1 next-to-NLO parton distribution function (PDF) set is used for simulating the hard processes.

To account for residual differences between the distributions of the multiplicity of PU vertices simulated in MC samples and those observed in data, a reweighting of MC events is performed. Photon identification efficiency and energy resolution are corrected for differences between data and simulation, as measured in $\mathrm{Z} \to \mathrm{e^+e^-}$ events [46], since photons and electrons are subject to similar reconstruction algorithms.

Simulated spin-1 Z′ resonance signal samples with the Z′ boson decaying to Hγ are generated at LO based on the benchmark model proposed in Ref. [20]. Following the discussion in Ref. [20], the intrinsic fractional width of the Z′ signal, $\Gamma_{Z'}/m_{Z'}$, is set to 0.01%, which is negligible compared to the detector resolution effects.

The model used to simulate the $Z\gamma$ resonance signal is a spin-0 heavy Higgs boson (S) generated using PYTHIA at LO. Three resonance width hypotheses are considered, with fractional widths Γ_S/m_S of 0.014, 5.6, and 10%, as has been done in previous analyses, allowing for a direct comparison. The simulation assumes no interference between the signal and the SM nonresonant $Z\gamma$ production.

For both Z′ and S boson signal scenarios and all width hypotheses, fully simulated signal samples are generated for 14 resonance masses. These are produced across the mass range 700–3500 GeV, with step sizes of 100 GeV for 700–1000 GeV, 200 GeV for 1000–2600 GeV, and the final point at 3500 GeV. The $m_{j\gamma}$ spectra of the signal samples are modeled using a bifurcated double-sided Crystal Ball (DCB) function [53, 54], which provides a good description of the simulated distributions for all signal points. For the masses between the 14 simulated $m_{Z'}$and $m_S$points, the signal $m_{j\gamma}$ shape is obtained by smoothly interpolating the DCB function parameters using a cubic spline fit [55]. The signal modeling obtained from interpolation is validated through comparisons across several simulated signal samples. For the broad-width signal scenarios ($\Gamma_S/m_S = 5.6$, 10%), a significant fraction of the signal events are produced off-shell, spreading across the $m_{j\gamma}$ spectrum at values lower than the nominal m_S, as illustrated in the right plot of Fig. 3. To ensure that the DCB model accurately describes the signal for broad widths, only the on-shell part of the $m_{j\gamma}$ distribution is considered, i.e., the fraction of signal events within the $m_S \pm 0.33 m_S$ range. This on-shell portion of the signal, which is consistently well modeled by the DCB function across all scenarios, is employed in the fit and in the interpretation of the results. Modeling the full off-shell tail would require a more complex function and offers little sensitivity gain, as its shape resembles the background and is absorbed by the fit. The systematic uncertainties are also interpolated with a cubic spline to ensure a smooth evolution across all tested signal scenarios.

4 Event reconstruction

The primary interaction vertex (PV) is taken to be the vertex corresponding to the hardest scattering in the event, evaluated using tracking information alone, as described in Section 9.4.1 of Ref. [56] and Ref. [57].

A particle-flow (PF) algorithm [58] aims to reconstruct and identify each interacting particle in an event, with an optimized combination of information from the various elements of the CMS detector. The energy of photons is obtained from the ECAL measurement. The energy of electrons is determined from a combination of the track momentum at the PV as determined by the tracker, the corresponding ECAL cluster energy, and the energy sum of all bremsstrahlung photons spatially compatible with originating from the electron track. The energy of muons is obtained from the corresponding track momentum. The energy of charged hadrons is determined from a combination of their momentum measured in the tracker and the matching ECAL and HCAL energy deposits, corrected for the response function of the calorimeters to hadronic showers. Finally, the energy of neutral hadrons is obtained from the corresponding corrected ECAL and HCAL energies.

For each event, hadronic jets are clustered from these reconstructed particles ("PF candidates") using the infrared- and collinear-safe anti-k_T jet clustering algorithm [59, 60], as implemented in the FASTJET package [60]. The clustering algorithm is run twice over the same inputs with the distance parameters 0.4 and 0.8, resulting in AK4 and AK8 jet collections, respectively. Jet momentum is determined as the vectorial sum of all particle momenta in the jet, and is found from simulation to be, on average, within 5 to 10% of the true momentum over the entire p_{T} spectrum and detector acceptance [61].

Particles from PU interactions can contribute additional tracks and calorimetric energy depositions within the same or nearby bunch crossings, increasing the apparent jet momentum. The PU-per-particle identification algorithm [57, 62] is used to mitigate the effect of PU in AK8 jets at the reconstructed particle level, making use of local shape information, event PU properties, and tracking information. A local shape variable is defined, which distinguishes between collinear and soft diffuse distributions of other particles surrounding the particle under consideration. The former is attributed to particles originating from the hard scatter, and the latter to particles originating from PU interactions. Charged particles identified to be originating from PU vertices are discarded. For each neutral particle, the local shape variable is computed using the surrounding charged particles compatible with the PV within the tracker acceptance ($|\eta| < 2.5$), and using both charged and neutral particles in the region outside of the tracker coverage. The momenta of the neutral particles are then rescaled according to their probability to originate from the PV deduced from the local shape variable, thus superseding the need for jet-based PU corrections [57].

Jet energy corrections are derived from simulation to bring the measured response of jets to that of particle level jets on average. Measurements in data of the momentum balance in dijet, γ+jet, Z+jets, and multijet events are used to account for any residual differences in the jet energy scale (JES) between data and simulation [61]. When combining information from the entire detector, the jet energy resolution (JER) typically amounts to 15–20% at 30 GeV, 10% at 100 GeV, and 5% at 1 TeV [61]. Additional selection criteria are applied to each jet to remove jets potentially dominated by anomalous contributions from various subdetector components or reconstruction failures [63].

The AK4 jets originating from the hadronization of b-quarks are identified as "b-tagged" using the ML-based DEEPJET [64, 65] algorithm that uses tracks within the jet that are displaced from the PV, identified secondary vertices, jet kinematic variables, neutral PF candidates, and information related to the presence of soft leptons in the jet as inputs. A threshold on the DEEPJET score is used, corresponding to a 1% probability of misidentifying a light-flavor quark or a gluon (udsg) AK4 jet with $p_{\mathrm{T}} > 30$ GeV and $|\eta| < 2.5$ as a b quark jet, while maintaining approximately 83% signal efficiency.

The missing transverse momentum vector, $\vec{p}_{\mathrm{T}}^{\mathrm{miss}}$, is computed as the negative vector sum of the transverse momenta ($\vec{p}_{\mathrm{T}}$) of all the PF candidates in an event, and its magnitude is denoted as $p_{\mathrm{T}}^{\mathrm{miss}}$ [66]. The $\vec{p}_{\mathrm{T}}^{\mathrm{miss}}$ is modified to account for corrections to the energy scale of the reconstructed jets in the event. Anomalous high-$p_{\mathrm{T}}^{\mathrm{miss}}$ events can occur as a result of a variety of reconstruction failures, detector malfunctions, or noncollision backgrounds. Such events are rejected by criteria designed to identify more than 85–90% of spurious high-$p_{\mathrm{T}}^{\mathrm{miss}}$ events with a signal efficiency loss of less than 0.1% [66].

The AK8 jets arising from hadronic decays of H and Z bosons are identified using the GLOPART ML algorithm [33], which uses PF candidates and secondary vertices as inputs. The algorithm is trained to classify jets into a total of 314 distinct classes, and its output consists of a score for each class corresponding to the probability that the jet belongs to that class. This large jet classification model extends beyond the needs of this analysis, offering a comprehensive set of jet classes designed to support the broad and diverse CMS data analysis program. It leverages larger training data sets and more complex classification tasks to enhance the overall tagging performance, as demonstrated in Ref. [67]. The present analysis employs the mass-decorrelated implementation [68] of GLOPART. The identification of H and Z bosons uses the Xbb score, defined as the ratio of the $X \to b\overline{b}$ class score to the sum of five scores of categories corresponding to jets produced purely via QCD multijet processes and $X \to b\overline{b}$ jets. The PARTICLENET algorithm also outputs an estimate of the jet's mass, referred to as the regressed jet mass, m_{j}, which is used in this analysis for further discrimination between $b\overline{b}$-candidate jets and background jets.

Photon candidates are reconstructed from energy deposits in the ECAL, referred to as superclusters, using a clustering algorithm that groups deposits consistent with the expected electromagnetic shower shape and accounts for energy recovery from photon conversions and electron bremsstrahlung. Since the dominant background arises from prompt-photon production rather than misidentified photons, a "loose" identification working point [43] is used to maximize photon efficiency, albeit with a slightly higher misidentification rate. The identification relies on photon shower shape and isolation variables, computed from PF candidates within a cone of radius $\Delta R = \sqrt{(\Delta\eta)^2 + (\Delta\phi)^2} = 0.3$ around the photon, where ϕ is the azimuthal angle, with corrections applied for PU effects. Additionally, a conversion-safe electron veto [43] is applied. Further details on the reconstruction and identification can be found in Ref. [43]. The loose working point achieves approximately 90% efficiency, with weak p_{T} dependence, while reducing misidentified photon backgrounds by a factor of 7 and limiting their contribution to below 7% of the total background. Photon candidates are further required to satisfy additional criteria to suppress backgrounds from jets and electrons, using electromagnetic shower shape and isolation variables, hadronic activity, and the absence of a matching track, as detailed in Ref. [12].

In order to reject SM background events with prompt electrons and muons (collectively referred to as leptons), selection criteria are applied in order to distinguish isolated leptons from leptons arising from heavy-flavor decays. Isolated electron (muon) candidates are required to be within the geometrical acceptance, which is $|\eta| < 2.5$ (2.4), and have $p_{T} > 35$ (20) GeV. Identified isolated electrons and muons are then selected based on the nearby hadronic activity in the event using an isolation variable defined by summing the p_{T} of all PF candidates in a cone of radius $\Delta R = 0.3$ (0.4) around the electron (muon) track, employing a correction for the contribution of neutral particles from PU interactions. More details on lepton isolation can be found in Refs. [43, 44].

5 Event selection

5.1 Trigger

The data sample used for this analysis is collected using a set of single-photon triggers that select events with at least one g candidate within $|\eta| < 2.5$ and passing photon p_{T} thresholds of 165 or 175 GeV for data collected in 2016 and 200 GeV for 2017–2018. The efficiencies of these triggers are measured using unbiased data samples collected using triggers that select events with single muons. These single-photon triggers have an efficiency above 98% relative to the offline selection criteria described below, and are consistent between data and simulation across the full mass range and data set. Residual inefficiencies are taken into account as a systematic uncertainty, as discussed in Section 7. This choice of triggers is identical to that used in Refs. [10, 11], where further details can be found.

5.2 Event preselection

Events considered in this analysis are selected in two steps. The first step, referred to as preselection, applies a loose set of requirements for events with roughly signal-like kinematic features, and the resulting sample is used in optimization studies. A more stringent set of requirements, optimized for high sensitivity in the SRs, defines the sample used in the statistical analysis. The analysis focuses on AK8 jets from H or Z boson decays, hereafter referred to simply as "jets", while their regressed mass estimator, m_{j}, is likewise referred to as the jet mass.

The preselection requires exactly one photon in the region $|\eta_{\gamma}| < 1.44$ or $1.57 < |\eta_{\gamma}| < 2.5$ [43] with $p_{\mathrm{T}}^{\gamma} > 225\,\mathrm{GeV}$ that satisfies the identification conditions described in Section 4. In addition, the preselection requires events to have at least one jet with $p_{\mathrm{T}}^{\mathrm{j}} > 250\,\mathrm{GeV}$ and $m_{\mathrm{j}} > 30\,\mathrm{GeV}$ in the region $|\eta_{\mathrm{j}}| < 2.4$. For events with more than one selected jet (7% of the preselection), the jet with the highest Xbb score is chosen as the H or Z candidate, resulting in a 5–10% misidentification rate depending on the resonance mass. Events that contain at least one isolated lepton (as defined in Section 4) are rejected. Photons in the event are required to be separated from the jet using the requirement $\Delta R(\mathrm{j}, \gamma) > 1.1$, which ensures minimal overlap between the photon and jet.

A subdominant background contribution arises from SM processes involving top quarks, single top, and $\mathrm{t\bar{t}}$ production produced in association with a photon (collectively referred to as "Top+γ"). To suppress these backgrounds, events containing b-tagged AK4 jets satisfying the requirement $\Delta R(\mathrm{b}, \mathrm{j}_{\mathrm{AK4}}) > 1.2$, indicating spatial separation from the candidate $\mathrm{b\bar{b}}$ jet, are rejected at the preselection level.

The receiver operating characteristic (ROC) curves, shown on the left of Fig. 2, indicate the superior signal vs. background separation performance of the Xbb discriminator, as compared with other tagging algorithms used in previous CMS searches reported in Refs. [10, 69–71]. In the right of Fig. 2, the Xbb discriminant scores in simulated signal samples and the data are shown, along with the statistical significance metric $S/\sqrt{D}$ in the lower panel, where S and D are the signal and data event yields, respectively. Both plots in Fig. 2 use the preselection criteria, with the Z$'$ signals normalized to their benchmark cross sections times branching fraction ($\sigma\mathcal{B}$) values, while the S signals are normalized to $\sigma\mathcal{B} = 10$ fb.

The m_{j} and $m_{\mathrm{j}\gamma}$ spectra at the preselection level are compared between data and simulated background samples in Fig. 3. Six signal scenarios are overlaid, with four corresponding to the same mass, enabling a direct shape comparison among the simulated resonances. The lower panels show the $S/\sqrt{D}$ distributions.

5.3 Signal region and event categorization

The full selection criteria, which define the SRs of this analysis, are a more stringent set of optimized event selection requirements that are applied in addition to the preselection criteria.

In order to further suppress the QCD multijet background, photons are required to lie within the ECAL barrel region, corresponding to $|\eta_{\gamma}| < 1.44$. This requirement takes advantage of the fact that signal events with masses above 700 GeV predominantly yield central photons, whereas photons produced in QCD background processes are more commonly observed in the forward regions of the detector.

The $\mathrm{b\bar{b}}$ jet candidates from H and Z boson decays exhibit distinctive substructures compared to background jets, which are predominantly produced in QCD processes. This difference arises primarily from their two-pronged structure and the presence of secondary vertices from

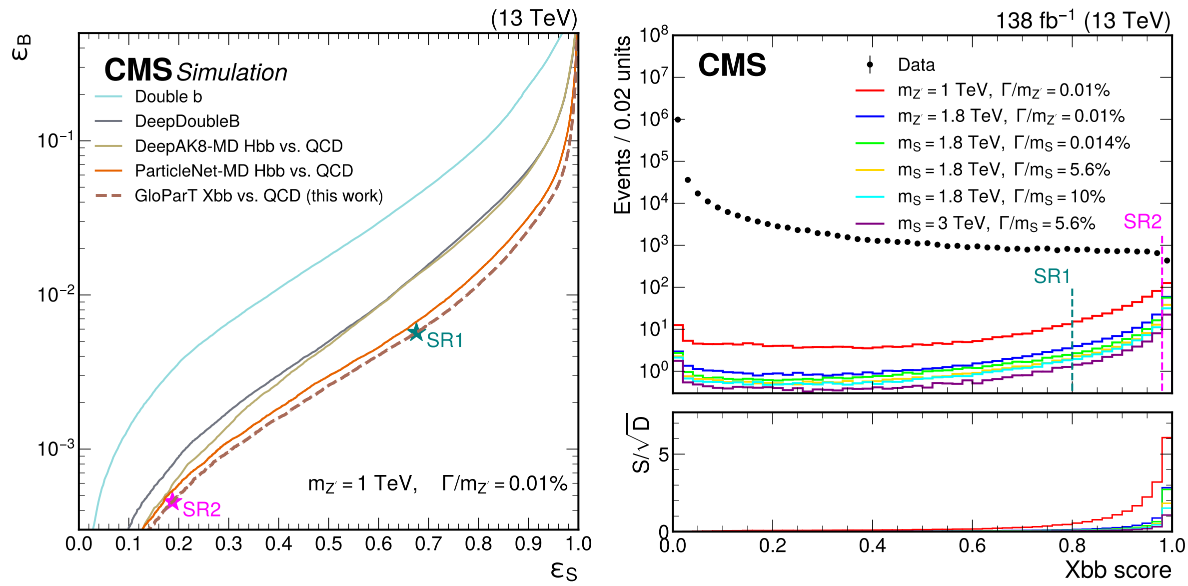

Figure 2: The ROC curves of background efficiency (ϵ_{B}) vs. signal efficiency (ϵ_{S}) for the Xbb tagger and other taggers from previous analyses, evaluated using a $m_{Z'} = 1$ TeV signal sample and SM background, are shown on the left. The taggers are listed in chronological order in the legend, based on their first use in similar searches (Refs. [10, 69–71]). The right plot shows the Xbb score distributions for data and simulated signal samples, along with the significance metric, $S/\sqrt{D}$, as defined in the text. Both plots use the preselection, with the Z′ (S) signals normalized by setting $\sigma\mathcal{B}$ to the benchmark values (10 fb).

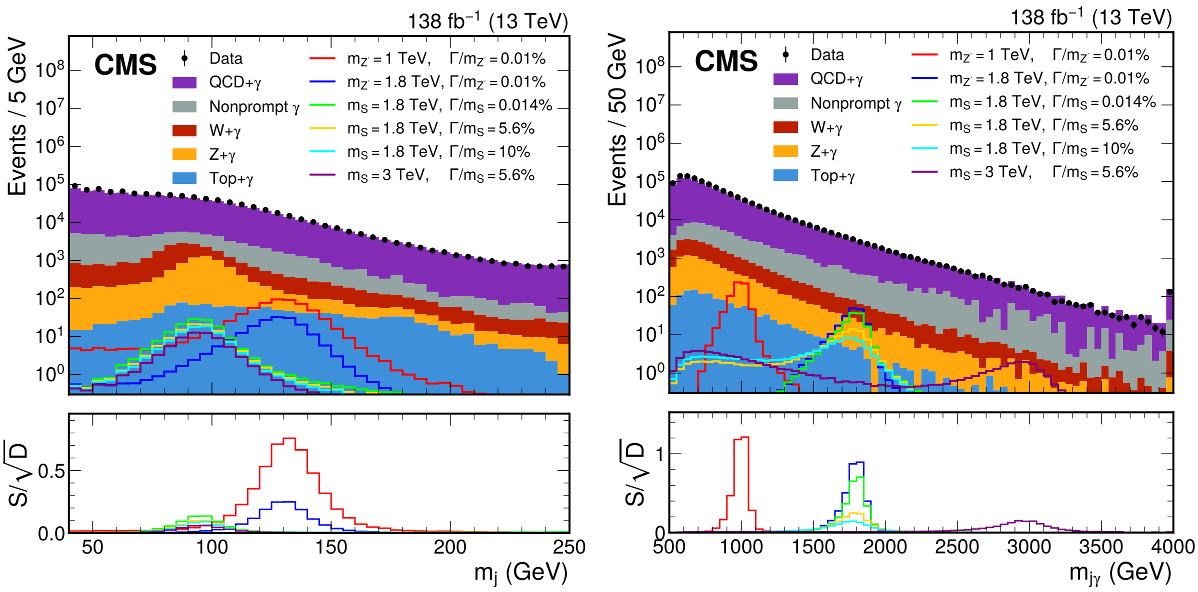

Figure 3: The left and right plots present the distributions of m_{j} and $m_{\mathrm{j}\gamma}$, respectively, in data, MC background, and signal samples, with preselection criteria applied. Both plots use the preselection, with the Z′ (S) signals normalized by setting $\sigma\mathcal{B}$ to the benchmark (10 fb) values.

b hadron decays. These features are effectively leveraged by the GLOPART algorithm through its dedicated Xbb tagger, which reliably assigns scores close to 1 for signal jets and close to 0 for background jets, as shown in the left plot of Fig. 2. The SR selection criteria include the requirement that Xbb > 0.8, which corresponds to a selection efficiency of approximately 68% (0.6)% for signal (background) jets, evaluated using the 1 TeV mass Z' resonance sample and the simulated background samples. Events meeting this criterion are further split into two categories based on the Xbb score—the first SR (SR1) requires $0.8 < \text{Xbb} < 0.98$, and the second SR (SR2) requires $0.98 < \text{Xbb} < 1$. The SR2 has high signal purity and provides most of the sensitivity, while SR1, with moderate purity, offers a complementary gain, especially at lower resonance masses where SR2 alone is less efficient. The Xbb boundary values of 0.8 and 0.98 were found to maximize the $S/\sqrt{D}$ across nearly all considered signal scenarios. The definitions of the SRs and the control regions (CRs) in the m_{j}-Xbb phase space are illustrated on the left of Fig. 4.

The SR requires $\text{b}\overline{\text{b}}$ candidate jets to have a mass in the range $80 < m_{\text{j}} < 150\,\text{GeV}$ to ensure compatibility with the nominal Z and H boson masses. Events are further categorized according to the value of m_{j}: those with m_{j} in the range 80–110 GeV are classified into the Z boson signal region (SRZ), while those in the 110–150 GeV range are classified into the Higgs boson signal region (SRH). This m_{j}-based categorization is applied in conjunction with the Xbb-based classification, resulting in four SRs, referred to as SRZ1, SRZ2, SRH1, and SRH2. The two regions labeled SRZ1 and SRZ2 target the $\text{S} \to \text{Z}\gamma$ signal, while SRH1 and SRH2 target the $\text{Z}' \to \text{H}\gamma$ signal. The product of signal selection efficiency and acceptance for each SR and signal scenario is shown on the right of Fig. 4.

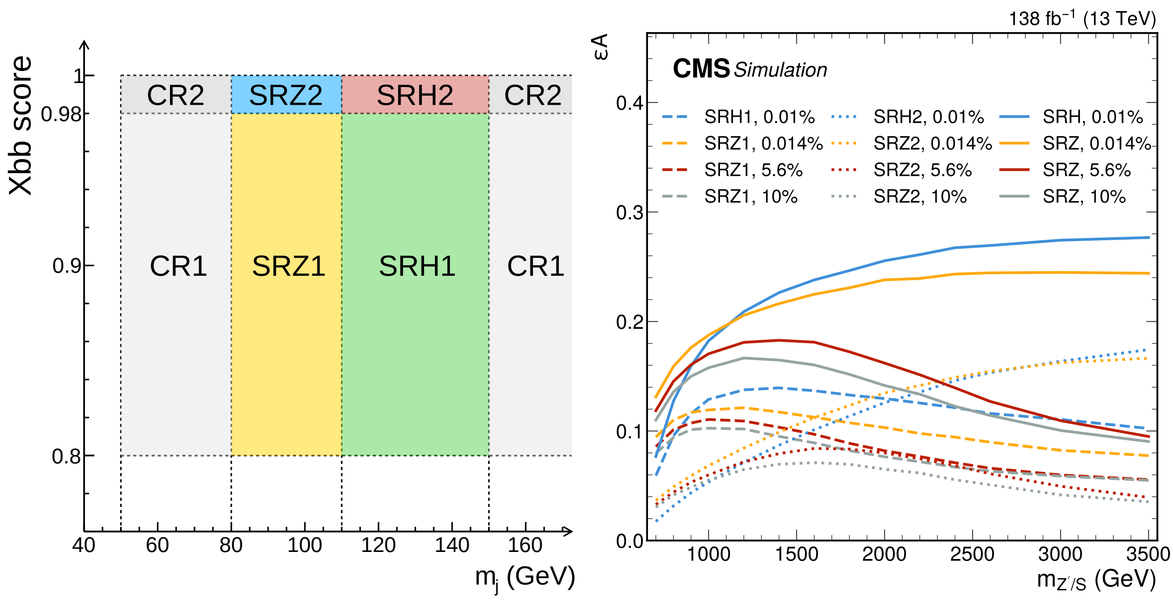

Figure 4: A schematic illustration of the SR and CR definitions in the m_{j}-Xbb plane is shown on the left. On the right, the product of signal efficiency and acceptance is plotted as a function of the resonance mass for the simulated signal samples in the relevant SRs. The percentages in the legend refer to the corresponding Γ/m values. Here, SRZ(H) denotes SRZ(H)1+SRZ(H)2.

The values that define the boundaries of SRZ and SRH are chosen such that the nominal masses of the H and Z bosons are not perfectly centered within the range. This decision is based on two factors. First, studies of the simulated signal samples indicate that their m_{j} distribution peaks approximately 4% higher than the nominal mass, primarily as a result of additional radiation captured within the jet cone. Second, the m_{j} distributions of the background MC samples are falling over the relevant m_{j} range, resulting in a larger background contribution to the SR when the lower boundary is chosen to be symmetric with the upper boundary, relative to the nominal H or Z masses. These effects are illustrated in the left plot of Fig. 3. Optimization studies demonstrate that the selected SRZ and SRH jet mass boundaries offer optimal sensitivity across all signal masses considered. All kinematic boundaries defining the SRs are chosen to maximize the $S/\sqrt{D}$ metric for both SRs and preselection event selections.

To define a CR with kinematic features similar to the SR, but expected to receive negligible contributions from possible signal processes, the CR selection criteria apply the same requirements as the SR, with the exception that the m_{j} requirement is inverted. Specifically, m_{j} is required to lie outside the SRH or SHZ ranges, $50 < m_{\mathrm{j}} < 80\,\text{GeV}$ or $m_{\mathrm{j}} > 150\,\text{GeV}$. This CR is then divided into two subregions, CR1 and CR2, based on the Xbb score, following the same categorization scheme as the SR. The CRs are not directly used in the statistical analysis, but are employed for optimization and validation studies, as discussed in Section 6.

The statistical analysis is performed using the $m_{\mathrm{j}\gamma}$ distributions in the four SRs (SRZ1, SRZ2, SRH1, and SRH2), as detailed in Section 6, while the CRs, though not used directly in the fit, are employed for optimization and validation.

5.4 Tagger calibration

In order to account for any differences in the performance of the Xbb tagger between the data and MC, a calibration procedure is carried out to derive compensating scale factors (SFs). This calibration is undertaken for each of the SR1 and SR2 regions using a dedicated data sample. The calibration of $\mathrm{Z,H} \rightarrow \mathrm{b\bar{b}}$ signal jets is performed using a dedicated sample of SM gluon-splitting jets, $\mathrm{g} \rightarrow \mathrm{b\bar{b}}$, which mimic signal jets and serve as proxies for them.

A boosted decision tree (BDT) classifier is used to select a high-purity sample of $\mathrm{g} \rightarrow \mathrm{b\bar{b}}$ jets from a QCD multijet-dominated event sample, based on substructure properties similar to those of the $\mathrm{Z,H} \rightarrow \mathrm{b\bar{b}}$ signal jets targeted for calibration. The SFs are derived by comparing the BDT-selected events in simulation to those in the data. These are applied to correct the jet selection efficiency in signal events. The derived SF values are binned by data-taking year, H candidate jet p_{T} (with the boundaries at 250, 400, and 600 GeV), and Xbb score matching the SRs (with boundaries at 0.8 and 0.98). The SF values range from 0.94 to 1.05 for SR1, and from 1.07 to 1.22 for SR2, with associated uncertainties of 2–12%. The same calibration method has been applied in several analyses [71–73]. Details for the calibration of $\mathrm{c\bar{c}}$ and $\mathrm{b\bar{b}}$ jet tagging, and the determination of their corresponding uncertainties, can be found in Refs. [74, 75].

6 Background modeling

Based on MC studies, it is observed that the background in SRZ1 and SRZ2 primarily arises from nonresonant SM QCD+γ and Z+γ processes (collectively about 96%), which dominate the low and high regions of the $m_{\mathrm{j}\gamma}$ spectra, respectively. Processes such as $\mathrm{t\bar{t}}$+γ, single t+γ, W+γ, as well as those involving misidentified photons, are highly suppressed, contributing to only about 4% of the selected events. Similarly, the background in the SRH1 and SRH2 regions consists predominantly of events from QCD+γ (about 84%), followed by Z+γ processes (10%), with the remaining 6% attributed to various other SM processes.

To avoid MC limitations and potential residual mismodeling, an approach based on data is used to model the background. This technique relies on creating the SM background prediction by directly fitting a set of smooth, monotonically falling functions to the $m_{\mathrm{j}\gamma}$ spectra in the data, independently in each of the four SRs.

A set of six functional forms of the $m_{j\gamma}$ variable is considered for performing this background fit and is employed in the statistical analysis:

$$\begin{aligned}
f_1(m) &= p_0 m^{p_1+p_2\log(m)} && \text{(Dijet2)},\\
f_2(m) &= p_0 m^{p_1+p_2\log(m)+p_3\log^2(m)} && \text{(Dijet3)},\\
f_3(m) &= p_0 m^{p_1} && \text{(ExPow1)},\\
f_4(m) &= p_0 m^{p_1} e^{p_2 m} && \text{(ExPow2)},\\
f_5(m) &= p_0 (1+p_1 m)^{p_2} && \text{(InvPow2)},\\
f_6(m) &= p_0 (1+p_1 m)^{p_2+p_3 m} && \text{(InvPow3)},
\end{aligned} \tag{1}$$

where m is defined as $m = m_{j\gamma}/\sqrt{s}$ and p_i are parameters constrained in the fit. The signal strength is extracted through an unbinned maximum likelihood fit using a profile likelihood test statistic [76]. To metigate uncertainty and bias arising from the choice of functional form, a discrete profiling technique [77–79] is employed. In this approach, the fit function is treated as a discrete nuisance parameter and profiled simultaneously with the continuous ones, to determine the optimal combination of background models for each signal mass hypothesis. This enables different functions, or combinations of those provided, to be selected in different regions of the likelihood parameter space, mitigating the bias from using a single functional form across the entire fit range.

The functional forms chosen for the background fit have been employed in numerous analyses involving two final-state physics objects, including dijet, diphoton, and photon+jet systems (e.g., [9–12, 80, 81]). These families of functions are validated using data in the CRs, as well as the MC background samples in both the CRs and SRs. These validation studies consistently demonstrate a good description of the observed $m_{j\gamma}$ spectra in all cases. The plots on the left and right of Fig. 5 show the $m_{j\gamma}$ spectra of the data in CR1 and CR2, respectively, together with the fit results. Each plot also shows the corresponding χ^2/ndf value (where the ndf is the number of degrees of freedom, ranging 63–65) used to quantify the fit quality. The indicated uncertainties on the data, σ_{stat}, represent Poisson statistical uncertainties. The systematic uncertainty shown, σ_{syst}, corresponds to an overlay of all six fit functions' statistical uncertainties, while the σ_{stat} is obtained directly from the data. The lower panels show the pull distributions, defined as the difference between the observed and predicted event yields from the best-fit function, divided by σ_{stat}. They also display the ratios of σ_{syst} to σ_{stat}.

The potential bias on the estimated signal significance arising from the chosen background parameterization is tested following the approach of Refs. [10, 80, 82], by generating pseudo-datasets and computing significances with the background function either fixed to that used in the generation or allowed to float in the fit. In all cases, no significant bias is induced.

7 Systematic uncertainties

Systematic uncertainties are considered for both background estimation and signal extraction. Each source of uncertainty is modeled with a nuisance parameter. These are listed in Table 1. The table also specifies whether an uncertainty affects the shape of the $m_{j\gamma}$ spectrum or the rate of a given process. The potential bias from using only six functional forms in the fit is negligible, based on MC studies and results from similar analyses [9–12].

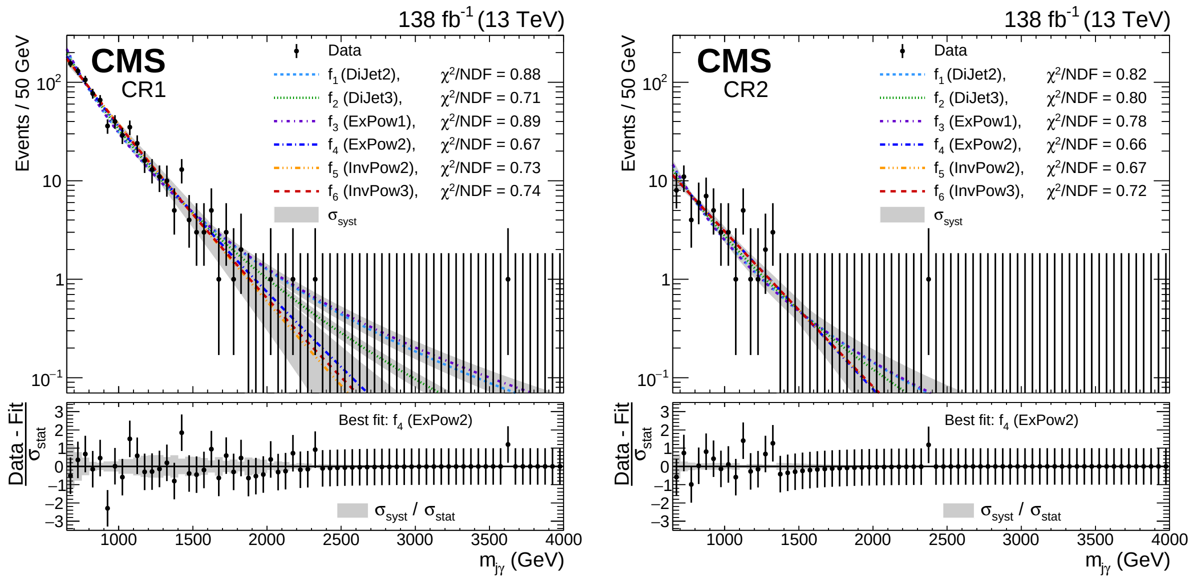

Figure 5: The $m_{j\gamma}$ distributions of the data in CR1 (left) and CR2 (right) fitted with the six parametric functions. The legends specify the χ^2/ndf for each fit. The lower panels show the pull distributions as defined in the text, with respect to the best fit function specified in the legend.

Table 1: The sources of systematic uncertainties included in the analysis. The second column indicates whether the uncertainty affects the background or signal shape or its rate. The third column from the left lists the magnitude of the corresponding pre-fit systematic uncertainty. The last column indicates the total number of nuisance parameters (NPs) and whether or not they are treated as correlated across all SRs. An asterisk (*) denotes a value or shape template unique to each signal scenario.

Uncertainty source	Effect on	Magnitude	Number of NPs & correlations
Background function choice	Shape	—	1 per SR, uncorr. across SRs
Photon identification SFs	Rate	4.4%	1, correlated across all SRs
Trigger selection SFs	Rate	1%	1, correlated across all SRs
Integrated luminosity	Rate	1.6%	1, correlated across all SRs
PU reweighting	Rate	1%	1, correlated across all SRs
PDFs	Rate	0.3–5.0%	1, correlated across all SRs *
μ_R and μ_F scales	Rate	0.2–1.2%	1, correlated across all SRs *
Xbb tagger SF systematic	Rate	3–7%	2, uncorr. across SRs *
Xbb tagger SF statistical	Rate	<4%	6, uncorr. across years and SRs *
JES	Shape	0.7–4.0% on the peak position	1, per data-taking year *
JER	Shape	0.5–4.0% on the peak width	1, correlated across SRs *
PES	Shape	0.3–0.7% on the peak position	1, correlated across SRs
PER	Shape	0.3–0.8% on the peak width	1, correlated across SRs

7.1 Systematic uncertainties in the background estimation

As described in Section 6, the uncertainty associated with the choice of the background fit function is accounted for in the discrete profiling method by treating the choice of the background fit function as a discrete nuisance parameter, which is profiled in a manner analogous to the continuous nuisance parameters in the statistical analysis. This approach minimizes potential bias in the fit function by relying on data to evaluate both the rate and shape of the predicted spectra.

7.2 Systematic uncertainties in the signal rate

The uncertainty in the integrated luminosity for the 2016, 2017, and 2018 data-taking periods is 1.2–2.5% [34–36], with an overall uncertainty of 1.6% for the entire 2016–2018 period. Uncertainty introduced by the PU reweighting procedure is assessed by varying the total inelastic cross section (assumed to be 69.2 mb) by $\pm$4.6% [83], leading to a 1% uncertainty in signal normalization in the SRs. It is observed that this variation has a negligible effect on the shape of the signals' $m_{j\gamma}$ distributions. Both the integrated luminosity uncertainty and the PU reweighting uncertainty are incorporated in the statistical analysis as nuisance parameters of log-normal type [76], hereafter referred to as log-normal priors.

Uncertainties of 4.4 and 1.0% from photon identification and trigger efficiency, respectively, are included based on data-to-simulation comparisons. They are treated as correlated across all signal regions and data-taking years, and are modeled with log-normal prior nuisance parameters.

The renormalization (μ_R) and factorization (μ_F) scale uncertainties, along with PDF uncertainties affecting signal acceptance, are evaluated independently for each SR and signal scenario. Scale uncertainties are derived by varying μ_R and μ_F independently by factors of 1/2 and 2, excluding extreme opposite-direction variations. Half of the maximum difference from these variations is assigned as the uncertainty, modeled with a log-normal prior, resulting in a $<$1.2% effect on the signal rate. The PDF uncertainties are evaluated using replicas of the NNPDF set and are applied to the selection acceptance for each signal scenario. Elements of the Hessian matrix are varied, and the quadratic sum of deviations from the central value is computed for each SR. The resulting variation in signal yields ranges from 0.3–5.1% across all signals considered. One nuisance parameter accounts for combined μ_R and μ_F uncertainties, and another for PDF variations. Both are treated with log-normal priors.

7.3 Systematic uncertainties in the signal shape

The JES uncertainty is assessed by varying the reconstructed four-momenta of all jets in an event based on their η- and p_T-dependent uncertainties. The resulting effect on the $m_{j\gamma}$ distributions is taken as the uncertainty. To account for differences in JER between data and simulation, smearing is applied to the latter, with jet resolutions varied according to their uncertainties. Both sources of uncertainty are modeled using nuisance parameters affecting the signals' $m_{j\gamma}$ spectra, with Gaussian priors. The effects of the photon energy scale (PES) and resolution (PER) are treated as uncertainties affecting only the signal shape, as their effects on signal rates were found to be negligible. These effects are considerably less significant than those arising from JES and JER due to the higher precision of photon energy reconstruction [43].

7.4 Systematic uncertainties in the Xbb tagger selection

Uncertainties in the Xbb tagger calibration, i.e., the derived SFs, are evaluated and summarized in Table 1. The dominant one arises from comparing SFs derived using two reweighting variations addressing mismodelling in the BDT score and the fit variable with the nominal result [74, 75]. The associated SF systematic uncertainty ranges from 3–7% for Z and H boson candidate jets, accounting for residual jet shower mismodeling. A different nuisance parameter is assigned for SR1 and SR2, each correlated across all data-taking years. Statistical uncertainties in the SFs, arising from limited sample sizes, 1–4%, are treated with separate nuisances per SR and data-taking year. A log-normal prior is used for all nuisance parameters. The impact on the $m_{j\gamma}$ shape is found to be negligible.

8 Statistical analysis and results

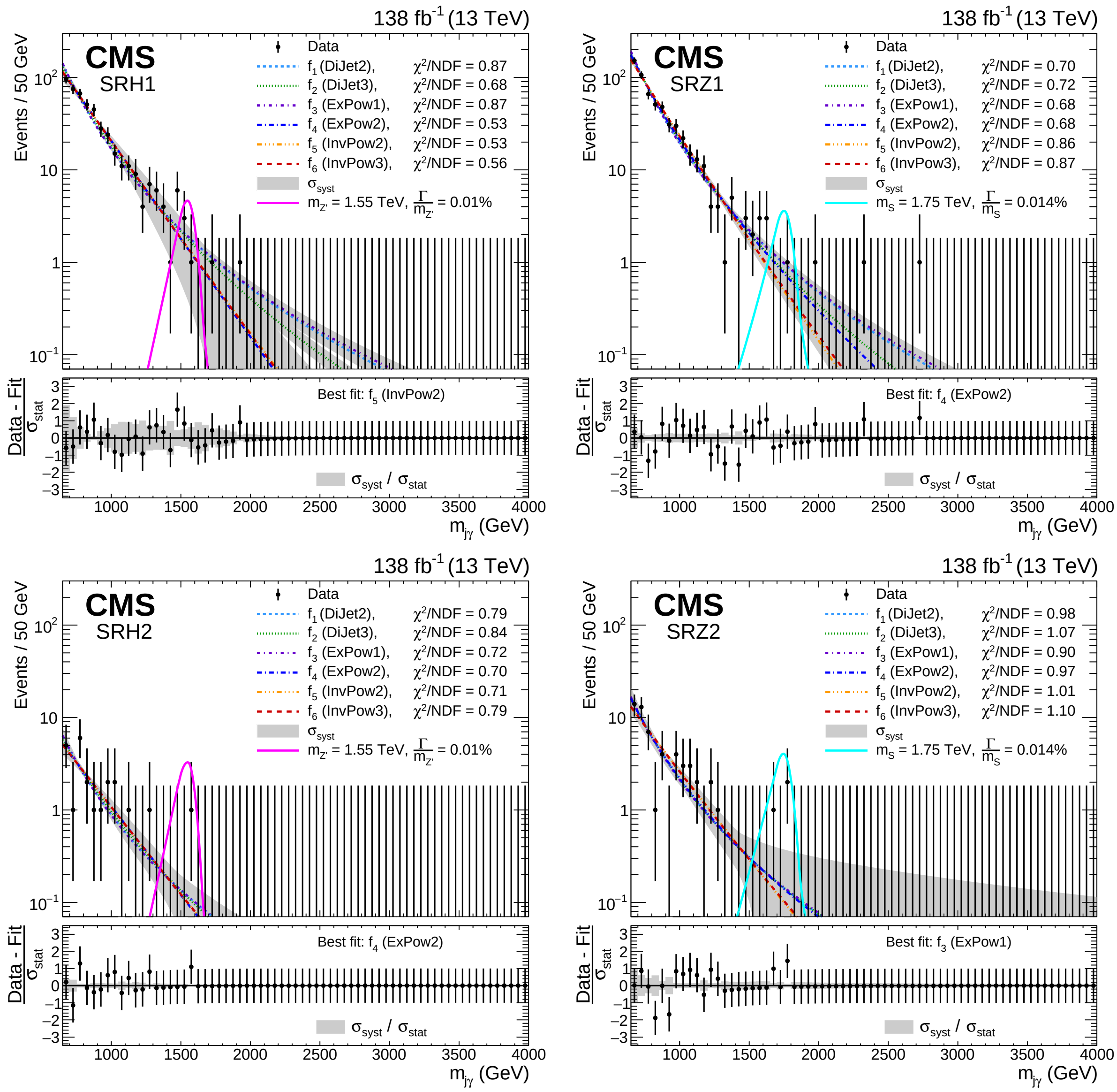

Figure 6: Post-fit $m_{j\gamma}$ spectra in the four SRs: SRH1 (upper left), SRZ1 (upper right), SRH2 (lower left), and SRZ2 (lower right). The legends specify the χ^2/ndf for each fit. The lower panels show the pull distributions with respect to the best fit function specified in the legend. The signals with the largest local significances are shown with continuous lines in each SR and are normalized to the observed $\sigma\mathcal{B}$ upper limits.

As described in Section 6, the search for Z′ and S resonances is conducted using an unbinned maximum likelihood fit to the $m_{j\gamma}$ distribution across all four SRs. The results, determined using the CMS statistical analysis tool COMBINE [76], are shown in Fig. 6, where for illustration purposes the data are shown with 50 GeV binning. No data events are observed beyond the displayed $m_{j\gamma}$ range. The data agree with the SM background prediction fit functions within the uncertainties.

The uncertainty in the background model arises from the limited number of data events at high $m_{j\gamma}$, which affects both the precision of the fit parameters and the choice of functional form. For the signal model, the dominant sources of systematic uncertainty are the Xbb tagger SF calibration and the JES. In the lower panels of Fig. 6, the ratio of systematic to statistical uncertainties, $\sigma_{syst}/\sigma_{stat}$, indicates the ranges where the uncertainty is dominated by the functional forms used in the fit or by the observed number of data events.

Upper limits at 95% confidence level (CL) are set on the product of the cross section and branching fraction ($\sigma\mathcal{B}$) for potential resonance signals as functions of $m_{Z'}$ and m_S, shown in Fig. 7. The limits are derived using the CL_s criterion [84, 85], based on a profile likelihood ratio test statistic in the LHC-style convention [76], modified for upper limit setting and evaluated using the asymptotic approximation [86].

For large widths, the limits weaken at high masses because a significant fraction of signal events are produced off-shell, as illustrated in the right panel of Fig. 3, leading to softer photons or jets than those selected. Furthermore, in the broad-width scenarios, only the on-shell component of the $m_{j\gamma}$ distribution within a window of $\pm 0.33 m_S$ around the nominal resonance mass is considered, where the DCB model remains valid.

This search excludes, at 95% CL, Z′ resonances decaying to H and a photon, with $m_{Z'}$in the range of 0.7–3.5 TeV, based on the benchmark model proposed in Ref. [20]. The observed limits on $\sigma\mathcal{B}$ set by this analysis are the most stringent to date for the benchmark Z′ model across the full mass range probed, surpassing previous best results from ATLAS [21] by roughly a factor of 3 and improving upon earlier CMS results [10] based on 2016 data by a factor of 6–10. For the H-like scalar S, the observed limits provide the most stringent constraints to date on $\sigma\mathcal{B}$ for $m_S > 1.2$ TeV, surpassing those reported by ATLAS in Ref. [87].

9 Summary

A search for heavy resonances decaying to a photon and a Z or a Higgs boson (H) in the γ+jet final state, using $\sqrt{s} = 13$ TeV proton-proton collision data collected with the CMS detector in 2016–2018, corresponding to an integrated luminosity of 138 fb^{-1}, has been presented. For the Hγ resonance analysis, a benchmark spin-1 resonance model with a narrow width is considered, while the Zγ analysis considers a standard model Higgs-like heavy spin-0 resonance, using several different width hypotheses. The final states of these resonant processes feature a photon and a massive, large-radius jet, containing the decay products of $H, Z \to b\overline{b}$, identified using the particle transformer jet substructure algorithm GLOPART for jet classification and the PARTICLENET algorithm for jet mass regression. These advanced machine-learning techniques greatly improve sensitivity over previous searches. The results are consistent with the predictions of the standard model within the measurement uncertainties. Exclusion limits at 95% confidence level are set on the product of the production cross section and the branching fraction for the resonance decay into Hγ or Zγ, with observed values below 0.1 and 0.3 fb for the spin-1 and spin-0 scenarios, respectively. This result establishes the most stringent constraints to date on the production and relevant decay of such heavy resonances.

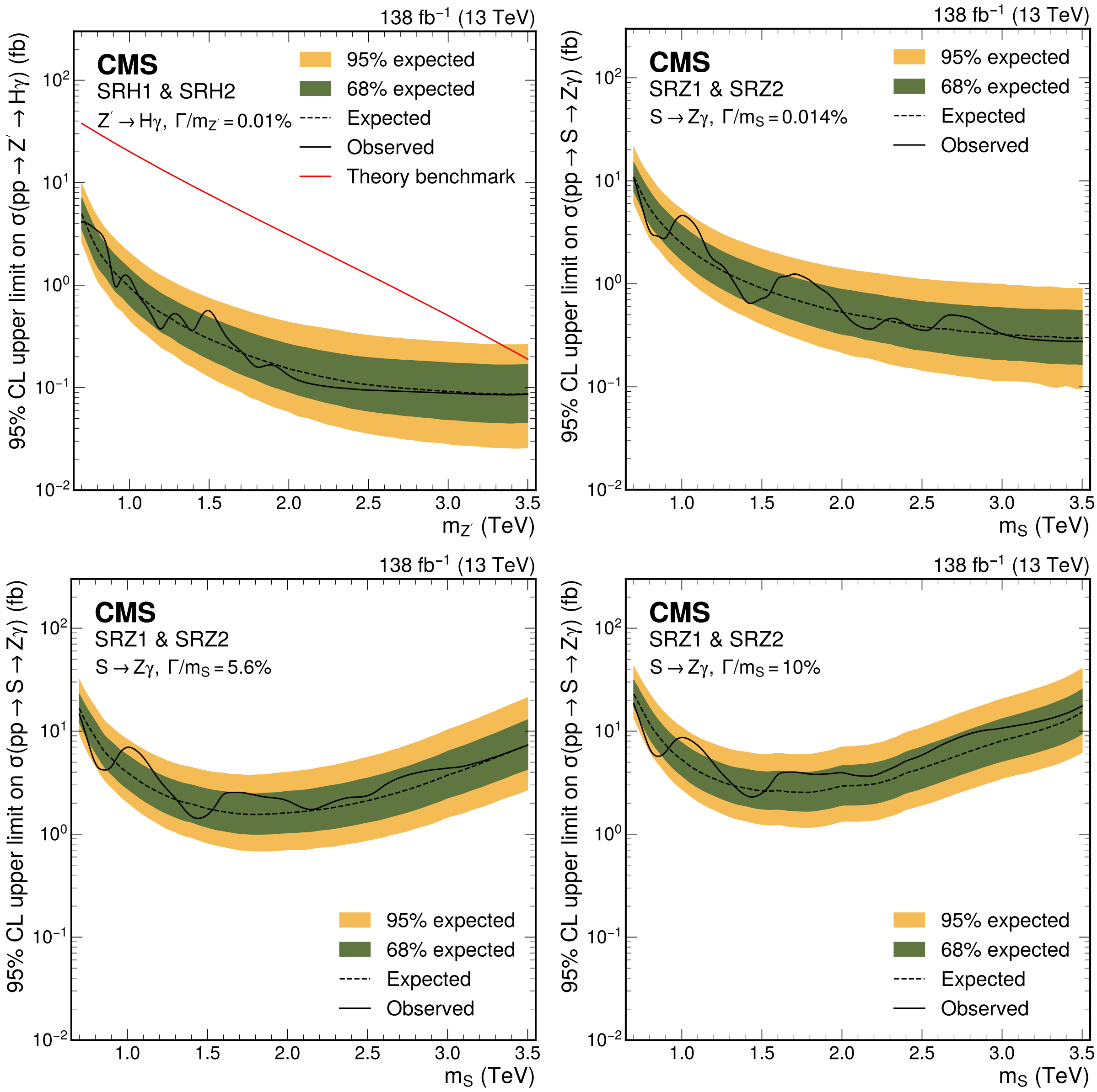

Figure 7: The 95% CL upper limits on the product of production cross section and branching fraction $\sigma\mathcal{B}$ for $Z' \to H\gamma$ (upper left) and $S \to Z\gamma$ with a narrow width (upper right), 5.6% width (lower left), and 10% width (lower right). Observed (expected) limits are shown with solid (dashed) lines. The colored bands represent the 68 and 95% CL intervals for the expected limits. The red line represents the theory benchmark model used for Z' signal simulation.

Acknowledgments

We congratulate our colleagues in the CERN accelerator departments for the excellent performance of the LHC and thank the technical and administrative staffs at CERN and at other CMS institutes for their contributions to the success of the CMS effort. In addition, we gratefully acknowledge the computing centers and personnel of the Worldwide LHC Computing Grid and other centers for delivering so effectively the computing infrastructure essential to our analyses. Finally, we acknowledge the enduring support for the construction and operation of the LHC, the CMS detector, and the supporting computing infrastructure provided by the following funding agencies: SC (Armenia), BMBWF and FWF (Austria); FNRS and FWO (Belgium); CNPq, CAPES, FAPERJ, FAPERGS, and FAPESP (Brazil); MES and BNSF (Bulgaria); CERN; CAS, MoST, and NSFC; MINCIENCIAS (Colombia); MSES and CSF (Croatia); RIF (Cyprus); SENESCYT (Ecuador); ERC PRG, TARISTU24-TK10 and MoER TK202 (Estonia); Academy of Finland, MEC, and HIP (Finland); CEA and CNRS/IN2P3 (France); SRNSF (Georgia); BMFTR, DFG, and HGF (Germany); GSRI (Greece); NKFIH (Hungary); DAE and DST (India); IPM (Iran); SFI (Ireland); INFN (Italy); MSIT and NRF (Republic of Korea); MES (Latvia); LMTLT (Lithuania); MOE and UM (Malaysia); BUAP, CINVESTAV, CONACYT, LNS, SEP, and UASLP-FAI (Mexico); MOS (Montenegro); MBIE (New Zealand); PAEC (Pakistan); MES, NSC, and NAWA (Poland); FCT (Portugal); MESTD (Serbia); MICIU/AEI and PCTI (Spain); MOSTR (Sri Lanka); Swiss Funding Agencies (Switzerland); MST (Taipei); MHESI (Thailand); TUBITAK and TENMAK (Türkiye); NASU (Ukraine); STFC (United Kingdom); DOE and NSF (USA).

Individuals have received support from the Marie-Curie program and the European Research Council and Horizon 2020 Grant, contract Nos. 675440, 724704, 752730, 758316, 765710, 824093, 101115353, 101002207, 101001205, and COST Action CA16108 (European Union); the Leventis Foundation; the Alfred P. Sloan Foundation; the Alexander von Humboldt Foundation; the Science Committee, project no. 22rl-037 (Armenia); the Fonds pour la Formation à la Recherche dans l'Industrie et dans l'Agriculture (FRIA) and Fonds voor Wetenschappelijk Onderzoek contract No. 1228724N (Belgium); the Beijing Municipal Science & Technology Commission, No. Z191100007219010, the Fundamental Research Funds for the Central Universities, the Ministry of Science and Technology of China under Grant No. 2023YFA1605804, the Natural Science Foundation of China under Grant No. 12061141002, 12535004, and USTC Research Funds of the Double First-Class Initiative No. YD2030002017; the Ministry of Education, Youth and Sports (MEYS) of the Czech Republic; the Shota Rustaveli National Science Foundation, grant FR-22-985 (Georgia); the Deutsche Forschungsgemeinschaft (DFG), among others, under Germany's Excellence Strategy – EXC 2121 "Quantum Universe" – 390833306, and under project number 400140256 - GRK2497; the Hellenic Foundation for Research and Innovation (HFRI), Project Number 2288 (Greece); the Hungarian Academy of Sciences, the New National Excellence Program - ÚNKP, the NKFIH research grants K 131991, K 133046, K 138136, K 143460, K 143477, K 146913, K 146914, K 147048, 2020-2.2.1-ED-2021-00181, TKP2021-NKTA-64, and 2021-4.1.2-NEMZ_KI-2024-00036 (Hungary); the Council of Science and Industrial Research, India; ICSC – National Research Center for High Performance Computing, Big Data and Quantum Computing, FAIR – Future Artificial Intelligence Research, and CUP I53D23001070006 (Mission 4 Component 1), funded by the NextGenerationEU program (Italy); the Latvian Council of Science; the Ministry of Education and Science, project no. 2022/WK/14, and the National Science Center, contracts Opus 2021/41/B/ST2/01369, 2021/43/B/ST2/01552, 2023/49/B/ST2/03273, and the NAWA contract BPN/PPO/2021/1/00011 (Poland); the Fundação para a Ciência e a Tecnologia, grant CEECIND/01334/2018 (Portugal); the National Priorities Research Program by Qatar National Research Fund; MICIU/AEI/10.13039/501100011033, ERDF/EU, "European Union NextGenerationEU/PRTR", and Programa Severo Ochoa del Principado de Asturias (Spain); the Chulalongkorn Academic into Its 2nd Century Project Advancement Project, the National Science, Research and Innovation Fund program IND_FF_68_369_2300_097, and the Program Management Unit for Human Resources & Institutional Development, Research and Innovation, grant B39G680009 (Thailand); the Kavli Foundation; the Nvidia Corporation; the SuperMicro Corporation; the Welch Foundation, contract C-1845; and the Weston Havens Foundation (USA).

References

[1] CMS Collaboration, "Search for heavy resonances decaying to $Z(\nu\bar{\nu})V(q\bar{q}')$ in proton-proton collisions at $\sqrt{s}$ = 13 TeV", *Phys. Rev. D* **106** (2022) 012004, doi:10.1103/PhysRevD.106.012004, arXiv:2109.08268.

[2] CMS Collaboration, "Search for new heavy resonances decaying to WW, WZ, ZZ, WH, or ZH boson pairs in the all-jets final state in proton-proton collisions at $\sqrt{s} = 13$ TeV", *Phys. Lett. B* **844** (2023) 137813, doi:10.1016/j.physletb.2023.137813, arXiv:2210.00043.

[3] CMS Collaboration, "Search for heavy resonances decaying to WW, WZ, or WH boson pairs in the lepton plus merged jet final state in proton-proton collisions at $\sqrt{s}$ = 13 TeV", *Phys. Rev. D* **105** (2022) 032008, doi:10.1103/PhysRevD.105.032008, arXiv:2109.06055.

[4] CMS Collaboration, "Search for high mass dijet resonances with a new background prediction method in proton-proton collisions at $\sqrt{s} = 13$ TeV", *JHEP* **05** (2020) 033, doi:10.1007/JHEP05(2020)033, arXiv:1911.03947.

[5] CMS Collaboration, "Search for a heavy resonance decaying into a Z and a Higgs boson in events with an energetic jet and two electrons, two muons, or missing transverse momentum in proton-proton collisions at $\sqrt{s}$ = 13 TeV", *JHEP* **02** (2025) 089, doi:10.1007/JHEP02(2025)089, arXiv:2411.00202.

[6] CMS Collaboration, "Search for heavy resonances decaying to ZZ or ZW and axion-like particles mediating nonresonant ZZ or ZH production at $\sqrt{s}$ = 13 TeV", *JHEP* **04** (2022) 087, doi:10.1007/JHEP04(2022)087, arXiv:2111.13669.

[7] CMS Collaboration, "Search for a heavy vector resonance decaying to a Z boson and a Higgs boson in proton-proton collisions at $\sqrt{s} = 13$ TeV", *Eur. Phys. J. C* **81** (2021) 688, doi:10.1140/epjc/s10052-021-09348-6, arXiv:2102.08198.

[8] CMS Collaboration, "Searches for Higgs boson production through decays of heavy resonances", *Phys. Rept.* **1115** (2025) 368, doi:10.1016/j.physrep.2024.09.004, arXiv:2403.16926.

[9] CMS Collaboration, "Search for $Z\gamma$ resonances using leptonic and hadronic final states in proton-proton collisions at $\sqrt{s} = 13$ TeV", *JHEP* **09** (2018) 148, doi:10.1007/JHEP09(2018)148, arXiv:1712.03143.

[10] CMS Collaboration, "Search for narrow $H\gamma$ resonances in proton-proton collisions at $\sqrt{s} = 13$ TeV", *Phys. Rev. Lett.* **122** (2019) 081804, doi:10.1103/PhysRevLett.122.081804, arXiv:1808.01257.

[11] CMS Collaboration, "Search for Wγ resonances in proton-proton collisions at $\sqrt{s} = 13$ TeV using hadronic decays of Lorentz-boosted W bosons", *Phys. Lett. B* **826** (2022) 136888, doi:10.1016/j.physletb.2022.136888, arXiv:2106.10509.

[12] CMS Collaboration, "Search for new physics in high-mass diphoton events from proton-proton collisions at $\sqrt{s}$ = 13 TeV", *JHEP* **08** (2024) 215, doi:10.1007/JHEP08(2024)215, arXiv:2405.09320.

[13] ATLAS Collaboration, "Search for resonances decaying into a weak vector boson and a Higgs boson in the fully hadronic final state produced in proton−proton collisions at $\sqrt{s} = 13$ TeV with the ATLAS detector", *Phys. Rev. D* **102** (2020) 112008, doi:10.1103/PhysRevD.102.112008, arXiv:2007.05293.

[14] ATLAS Collaboration, "Search for heavy diboson resonances in semileptonic final states in pp collisions at $\sqrt{s} = 13$ TeV with the ATLAS detector", *Eur. Phys. J. C* **80** (2020) 1165, doi:10.1140/epjc/s10052-020-08554-y, arXiv:2004.14636.

[15] ATLAS Collaboration, "Search for diboson resonances in hadronic final states in 139 fb^{-1} of pp collisions at $\sqrt{s} = 13$ TeV with the ATLAS detector", *JHEP* **09** (2019) 091, doi:10.1007/JHEP09(2019)091, arXiv:1906.08589. [Erratum: doi:10.1007/JHEP06(2020)042].

[16] ATLAS Collaboration, "Combination of searches for heavy spin-1 resonances using 139 fb^{-1} of proton-proton collision data at $\sqrt{s}$ = 13 TeV with the ATLAS detector", *JHEP* **04** (2024) 118, doi:10.1007/JHEP04(2024)118, arXiv:2402.10607.

[17] ATLAS Collaboration, "Search for resonant WZ production in the fully leptonic final state in proton–proton collisions at $\sqrt{s} = 13$ TeV with the ATLAS detector", *Eur. Phys. J. C* **83** (2023) 633, doi:10.1140/epjc/s10052-023-11437-7, arXiv:2207.03925.

[18] ATLAS Collaboration, "Search for heavy resonances decaying into a Z or W boson and a Higgs boson in final states with leptons and b-jets in 139 fb^{-1} of pp collisions at $\sqrt{s} = 13$ TeV with the ATLAS detector", *JHEP* **06** (2023) 016, doi:10.1007/JHEP06(2023)016, arXiv:2207.00230.

[19] ATLAS Collaboration, "Search for new resonances in mass distributions of jet pairs using 139 fb^{-1} of pp collisions at $\sqrt{s} = 13$ TeV with the ATLAS detector", *JHEP* **03** (2020) 145, doi:10.1007/JHEP03(2020)145, arXiv:1910.08447.

[20] B. A. Dobrescu, P. J. Fox, and J. Kearney, "Higgs–photon resonances", *Eur. Phys. J. C* **77** (2017) 704, doi:10.1140/epjc/s10052-017-5276-9, arXiv:1705.08433.

[21] ATLAS Collaboration, "Search for heavy resonances decaying into a photon and a hadronically decaying Higgs boson in pp collisions at $\sqrt{s} = 13$ TeV with the ATLAS detector", *Phys. Rev. Lett.* **125** (2020) 251802, doi:10.1103/PhysRevLett.125.251802, arXiv:2008.05928.

[22] E. Eichten and K. Lane, "Low-scale technicolor at the Tevatron and LHC", *Phys. Lett. B* **669** (2008) 235, doi:10.1016/j.physletb.2008.09.047, arXiv:0706.2339.

[23] A. Freitas and P. Schwaller, "Multi-photon signals from composite models at LHC", *JHEP* **01** (2011) 022, doi:10.1007/JHEP01(2011)022, arXiv:1010.2528.

[24] R. Barbieri and R. Torre, "Signals of single particle production at the earliest LHC", *Phys. Lett. B* **695** (2011) 259, doi:10.1016/j.physletb.2010.11.037, arXiv:1008.5302.

[25] I. Low, J. Lykken, and G. Shaughnessy, "Singlet scalars as Higgs imposters at the Large Hadron Collider", *Phys. Rev. D* **84** (2011) 035027, doi:10.1103/PhysRevD.84.035027, arXiv:1105.4587.

[26] H. Davoudiasl, J. L. Hewett, and T. G. Rizzo, "Experimental probes of localized gravity: On and off the wall", *Phys. Rev. D* **63** (2001) 075004, doi:10.1103/PhysRevD.63.075004, arXiv:hep-ph/0006041.

[27] B. C. Allanach, J. P. Skittrall, and K. Sridhar, "Z boson decay to photon plus Kaluza-Klein graviton in large extra dimensions", *JHEP* **11** (2007) 089, doi:10.1088/1126-6708/2007/11/089, arXiv:0705.1953.

[28] ATLAS Collaboration, "Search for heavy resonances decaying to a photon and a hadronically decaying $Z/W/H$ boson in pp collisions at $\sqrt{s} = 13$ TeV with the ATLAS detector", *Phys. Rev. D* **98** (2018) 032015, doi:10.1103/PhysRevD.98.032015, arXiv:2103.02708.

[29] ATLAS Collaboration, "Searches for the $Z\gamma$ decay mode of the Higgs boson and for new high-mass resonances in pp collisions at $\sqrt{s} = 13$ TeV with the ATLAS detector", *JHEP* **10** (2017) 112, doi:10.1007/JHEP10(2017)112, arXiv:1708.00212.

[30] H. Qu and L. Gouskos, "ParticleNet: Jet Tagging via Particle Clouds", *Phys. Rev. D* **101** (2020) 056019, doi:10.1103/PhysRevD.101.056019, arXiv:1902.08570.

[31] CMS Collaboration, "Mass regression of highly-boosted jets using graph neural networks", CMS Detector Performance Note CMS-DP-2021-017, 2021.

[32] A. J. Larkoski, S. Marzani, G. Soyez, and J. Thaler, "Soft drop", *JHEP* **05** (2014) 146, doi:10.1007/JHEP05(2014)146, arXiv:1402.2657.

[33] H. Qu, C. Li, and S. Qian, "Particle Transformer for Jet Tagging", *arXiv preprint* **162** (2022) doi:10.48550/arXiv.2202.03772, arXiv:2202.03772.

[34] CMS Collaboration, "Precision luminosity measurement in proton-proton collisions at $\sqrt{s} = 13$ TeV in 2015 and 2016 at CMS", *Eur. Phys. J. C* **81** (2021) 800, doi:10.1140/epjc/s10052-021-09538-2, arXiv:2104.01927.

[35] CMS Collaboration, "CMS luminosity measurement for the 2017 data-taking period at $\sqrt{s}$ = 13 TeV", CMS Physics Analysis Summary CMS-PAS-LUM-17-004, 2018.

[36] CMS Collaboration, "CMS luminosity measurement for the 2018 data-taking period at $\sqrt{s}$ = 13 TeV", CMS Physics Analysis Summary CMS-PAS-LUM-18-002, 2019.

[37] "HEPData record for this analysis", 2025. doi:10.17182/hepdata.158361.

[38] CMS Collaboration, "The CMS experiment at the CERN LHC", *JINST* **3** (2008) doi:10.1088/1748-0221/3/08/S08004, arXiv:0802.2978.

[39] CMS Collaboration, "Development of the CMS detector for the CERN LHC Run 3", *JINST* **19** (2024) P05064, doi:10.1088/1748-0221/19/05/P05064, arXiv:2309.05466.

[40] CMS Collaboration, "Performance of the CMS Level-1 trigger in proton-proton collisions at $\sqrt{s} = 13\,\text{TeV}$", *JINST* **15** (2020) P10017, doi:10.1088/1748-0221/15/10/P10017, arXiv:2006.10165.

[41] CMS Collaboration, "The CMS trigger system", *JINST* **12** (2017) P01020, doi:10.1088/1748-0221/12/01/P01020, arXiv:1609.02366.

[42] CMS Collaboration, "Performance of the CMS high-level trigger during LHC Run 2", *JINST* **19** (2024) P11021, doi:10.1088/1748-0221/19/11/P11021, arXiv:2410.17038.

[43] CMS Collaboration, "Electron and photon reconstruction and identification with the CMS experiment at the CERN LHC", *JINST* **16** (2021) P05014, doi:10.1088/1748-0221/16/05/P05014, arXiv:2012.06888.

[44] CMS Collaboration, "Performance of the CMS muon detector and muon reconstruction with proton-proton collisions at $\sqrt{s} = 13$ TeV", *JINST* **13** (2018) P06015, doi:10.1088/1748-0221/13/06/P06015, arXiv:1804.04528.

[45] CMS Collaboration, "Description and performance of track and primary-vertex reconstruction with the CMS tracker", *JINST* **9** (2014) P10009, doi:10.1088/1748-0221/9/10/P10009, arXiv:1405.6569.

[46] CMS Collaboration, "Performance of photon reconstruction and identification with the CMS detector in proton-proton collisions at $\sqrt{s} = 8$ TeV", *JINST* **10** (2015) P08010, doi:10.1088/1748-0221/10/08/P08010, arXiv:1502.02702.

[47] CMS Tracker Group Collaboration, "The CMS Phase-1 pixel detector upgrade", *JINST* **16** (2021) P02027, doi:10.1088/1748-0221/16/02/P02027, arXiv:2012.14304.

[48] CMS Collaboration, "Track impact parameter resolution for the full pseudo rapidity coverage in the 2017 dataset with the CMS Phase-1 pixel detector", CMS Detector Performance Summary CMS-DP-2020-049, 2020.

[49] J. Alwall et al., "The automated computation of tree-level and next-to-leading order differential cross sections, and their matching to parton shower simulations", *JHEP* **07** (2014) 079, doi:10.1007/JHEP07(2014)079, arXiv:1405.0301.

[50] T. Sjöstrand et al., "An introduction to PYTHIA 8.2", *Comput. Phys. Commun.* **191** (2015) 159, doi:10.1016/j.cpc.2015.01.024, arXiv:1410.3012.

[51] CMS Collaboration, "Extraction and validation of a new set of CMS PYTHIA8 tunes from underlying-event measurements", *Eur. Phys. J. C* **80** (2020) 4, doi:10.1140/epjc/s10052-019-7499-4, arXiv:1903.12179.

[52] GEANT4 Collaboration, "GEANT4—a simulation toolkit", *Nucl. Instrum. Meth. A* **506** (2003) 250, doi:10.1016/S0168-9002(03)01368-8.

[53] M. J. Oreglia, "A study of the reactions $\psi' \to \gamma\gamma\psi$". PhD thesis, Stanford University, 1980. SLAC Report SLAC-R-236.

[54] J. E. Gaiser, "Charmonium spectroscopy from radiative decays of the J/ψ and ψ'". PhD thesis, Stanford University, 1982. SLAC Report SLAC-R-255.

[55] A. L. Read, "Linear interpolation of histograms", *Nucl. Instrum. Meth. A* **425** (1999) 357, doi:10.1016/S0168-9002(98)01347-3.

[56] CMS Collaboration, "Technical proposal for the Phase-II upgrade of the Compact Muon Solenoid", CMS Technical Proposal CERN-LHCC-2015-010, CMS-TDR-15-02, 2015.

[57] CMS Collaboration, "Pileup mitigation at CMS in 13 TeV data", *JINST* **15** (2020) P09018, doi:10.1088/1748-0221/15/09/P09018, arXiv:2003.00503.

[58] CMS Collaboration, "Particle-flow reconstruction and global event description with the CMS detector", *JINST* **12** (2017) P10003, doi:10.1088/1748-0221/12/10/P10003, arXiv:1706.04965.

[59] M. Cacciari, G. P. Salam, and G. Soyez, "The anti-k_T jet clustering algorithm", *JHEP* **04** (2008) 063, doi:10.1088/1126-6708/2008/04/063, arXiv:0802.1189.

[60] M. Cacciari, G. P. Salam, and G. Soyez, "FastJet user manual", *Eur. Phys. J. C* **72** (2012) 1896, doi:10.1140/epjc/s10052-012-1896-2, arXiv:1111.6097.

[61] CMS Collaboration, "Jet energy scale and resolution in the CMS experiment in pp collisions at 8 TeV", *JINST* **12** (2017) P02014, doi:10.1088/1748-0221/12/02/P02014, arXiv:1607.03663.

[62] D. Bertolini, P. Harris, M. Low, and N. Tran, "Pileup per particle identification", *JHEP* **10** (2014) 059, doi:10.1007/JHEP10(2014)059, arXiv:1407.6013.

[63] CMS Collaboration, "Jet algorithms performance in 13 TeV data", CMS Physics Analysis Summary CMS-NOTE-2011-005, ATL-PHYS-PUB-2011-11, 2017.

[64] E. Bols et al., "Jet flavour classification using DeepJet", *JINST* **15** (2020) P12012, doi:10.1088/1748-0221/15/12/P12012, arXiv:2008.10519.

[65] CMS Collaboration, "Performance of the DeepJet b tagging algorithm using 41.9 fb^{-1} of data from proton-proton collisions at 13 TeV with Phase-1 CMS detector", CMS Detector Performance Note CMS-DP-2018-058, 2018.

[66] CMS Collaboration, "Performance of missing transverse momentum reconstruction in proton-proton collisions at $\sqrt{s} = 13$ TeV using the CMS detector", *JINST* **14** (2019) P07004, doi:10.1088/1748-0221/14/07/P07004, arXiv:1903.06078.

[67] C. Li et al., "Accelerating Resonance Searches via Signature-Oriented Pre-training", *Phys. Rev. D* **112** (2025) 015015, doi:10.1103/PhysRevD.112.015015, arXiv:2405.12972.

[68] CMS Collaboration, "Identification of highly Lorentz-boosted heavy particles using graph neural networks and new mass decorrelation techniques", CMS Detector Performance Note CMS-DP-2020-002, 2020.

[69] CMS Collaboration, "Inclusive search for highly boosted Higgs bosons decaying to bottom quark-antiquark pairs in proton-proton collisions at $\sqrt{s} = 13$ TeV", *JHEP* **12** (2020) 085, doi:10.1007/JHEP12(2020)085, arXiv:2006.13251.

[70] CMS Collaboration, "Search for heavy resonances decaying to a pair of Lorentz-boosted Higgs bosons in final states with leptons and a bottom quark pair at $\sqrt{s} = 13$ TeV", *JHEP* **05** (2022) 005, doi:10.1007/JHEP05(2022)005, arXiv:2112.03161.

[71] CMS Collaboration, "Search for nonresonant pair production of highly energetic Higgs bosons decaying to bottom quarks", *Phys. Rev. Lett.* **131** (2023) 041803, doi:10.1103/PhysRevLett.131.041803, arXiv:2205.06667.

[72] CMS Collaboration, "A search for the standard model Higgs boson decaying to charm quarks", *JHEP* **03** (2020) 131, doi:10.1007/JHEP03(2020)131, arXiv:1912.01662.

[73] CMS Collaboration, "Search for Higgs boson pair production with one associated vector boson in proton-proton collisions at $\sqrt{s}$ = 13 TeV", *JHEP* **10** (2024) 061, doi:10.1007/JHEP10(2024)061, arXiv:2404.08462.

[74] CMS Collaboration, "Calibration of the mass-decorrelated particlenet tagger for boosted $b\bar{b}$ and $c\bar{c}$ jets using LHC Run 2 data", CMS Detector Performance Note CMS-DP-2022-005, 2022.

[75] CMS Collaboration, "Performance of heavy-flavour jet identification in Lorentz-boosted topologies in proton-proton collisions at $\sqrt{s}$ = 13 TeV", 2025. arXiv:2510.10228. doi:10.1088/1748-0221/20/11/P11006.

[76] CMS Collaboration, "The CMS statistical analysis and combination tool: Combine", *Comput. Softw. Big Sci.* **8** (2024) 19, doi:10.1007/s41781-024-00121-4, arXiv:2404.06614.

[77] P. D. Dauncey, M. Kenzie, N. Wardle, and G. J. Davies, "Handling uncertainties in background shapes: the discrete profiling method", *JINST* **10** (2015) P04015, doi:10.1088/1748-0221/10/04/P04015, arXiv:1408.6865.

[78] CMS Collaboration, "Observation of the diphoton decay of the Higgs boson and measurement of its properties", *Eur. Phys. J. C* **74** (2014) 3076, doi:10.1140/epjc/s10052-014-3076-z, arXiv:1407.0558.

[79] ATLAS and CMS Collaboration, "Combined measurement of the Higgs boson mass in pp collisions at $\sqrt{s} = 7$ and 8 TeV with the ATLAS and CMS experiments", *Phys. Rev. Lett.* **114** (2015) 191803, doi:10.1103/PhysRevLett.114.191803, arXiv:1503.07589.

[80] CMS Collaboration, "Search for physics beyond the standard model in high-mass diphoton events from proton-proton collisions at $\sqrt{s} = 13$ TeV", *Phys. Rev. D* **98** (2018) 092001, doi:10.1103/PhysRevD.98.092001, arXiv:1809.00327.

[81] CMS Collaboration, "Search for resonant and nonresonant production of pairs of dijet resonances in proton-proton collisions at $\sqrt{s} = 13$ TeV", *JHEP* **07** (2023) 161, doi:10.1007/JHEP07(2023)161, arXiv:2206.09997.

[82] H. F. Tsoi et al., "SymbolFit: Automatic parametric modeling with symbolic regression", *Comput. Softw. Big Sci.* **9** (2025) 12, doi:10.1007/s41781-025-00140-4, arXiv:2411.09851.

[83] CMS Collaboration, "Measurement of the inelastic proton-proton cross section at $\sqrt{s} = 13$ TeV", *JHEP* **07** (2018) 161, doi:10.1007/JHEP07(2018)161, arXiv:1802.02613.

[84] T. Junk, "Confidence level computation for combining searches with small statistics", *Nucl. Instrum. Meth. A* **434** (1999) 435, doi:10.1016/S0168-9002(99)00498-2, arXiv:hep-ex/9902006.

[85] A. L. Read, “Presentation of search results: The CL_s technique”, *J. Phys. G* **28** (2002) 2693, doi:10.1088/0954-3899/28/10/313, arXiv:hep-ph/0203228.

[86] G. Cowan, K. Cranmer, E. Gross, and O. Vitells, “Asymptotic formulae for likelihood-based tests of new physics”, *Eur. Phys. J. C* **71** (2011) 1554, doi:10.1140/epjc/s10052-011-1554-0, arXiv:1007.1727. [Erratum: doi:10.1140/epjc/s10052-013-2501-z].

[87] ATLAS Collaboration, “Search for the $Z\gamma$ decay mode of new high-mass resonances in pp collisions at $\sqrt{s} = 13$ TeV with the ATLAS detector”, *Phys. Lett. B* **848** (2024) 138394, doi:10.1016/j.physletb.2023.138394, arXiv:2309.04364.

A The CMS Collaboration

Yerevan Physics Institute, Yerevan, Armenia
A. Hayrapetyan, V. Makarenko, A. Tumasyan[1]

Institut für Hochenergiephysik, Vienna, Austria
W. Adam, J.W. Andrejkovic, L. Benato, T. Bergauer, M. Dragicevic, C. Giordano, P.S. Hussain, M. Jeitler[2], N. Krammer, A. Li, D. Liko, M. Matthewman, I. Mikulec, J. Schieck[2], R. Schöfbeck[2], D. Schwarz, M. Shooshtari, M. Sonawane, W. Waltenberger, C.-E. Wulz[2]

Universiteit Antwerpen, Antwerpen, Belgium
T. Janssen, H. Kwon, D. Ocampo Henao, T. Van Laer, P. Van Mechelen

Vrije Universiteit Brussel, Brussel, Belgium
J. Bierkens, N. Breugelmans, J. D'Hondt, S. Dansana, A. De Moor, M. Delcourt, F. Heyen, Y. Hong, P. Kashko, S. Lowette, I. Makarenko, D. Müller, J. Song, S. Tavernier, M. Tytgat[3], G.P. Van Onsem, S. Van Putte, D. Vannerom

Université Libre de Bruxelles, Bruxelles, Belgium
B. Bilin, B. Clerbaux, A.K. Das, I. De Bruyn, G. De Lentdecker, H. Evard, L. Favart, P. Gianneios, A. Khalilzadeh, F.A. Khan, A. Malara, M.A. Shahzad, L. Thomas, M. Vanden Bemden, C. Vander Velde, P. Vanlaer, F. Zhang

Ghent University, Ghent, Belgium
M. De Coen, D. Dobur, G. Gokbulut, J. Knolle, D. Marckx, K. Skovpen, A.M. Tomaru, N. Van Den Bossche, J. van der Linden, J. Vandenbroeck, L. Wezenbeek

Université Catholique de Louvain, Louvain-la-Neuve, Belgium
S. Bein, A. Benecke, A. Bethani, G. Bruno, A. Cappati, J. De Favereau De Jeneret, C. Delaere, A. Giammanco, A.O. Guzel, V. Lemaitre, J. Lidrych, P. Malek, P. Mastrapasqua, S. Turkcapar

Centro Brasileiro de Pesquisas Fisicas, Rio de Janeiro, Brazil
G.A. Alves, M. Barroso Ferreira Filho, E. Coelho, C. Hensel, T. Menezes De Oliveira, C. Mora Herrera[4], P. Rebello Teles, M. Soeiro, E.J. Tonelli Manganote[5], A. Vilela Pereira[4]

Universidade do Estado do Rio de Janeiro, Rio de Janeiro, Brazil
W.L. Aldá Júnior, H. Brandao Malbouisson, W. Carvalho, J. Chinellato[6], M. Costa Reis, E.M. Da Costa, G.G. Da Silveira[7], D. De Jesus Damiao, S. Fonseca De Souza, R. Gomes De Souza, S. S. Jesus, T. Laux Kuhn[7], M. Macedo, K. Mota Amarilo, L. Mundim, H. Nogima, J.P. Pinheiro, A. Santoro, A. Sznajder, M. Thiel, F. Torres Da Silva De Araujo[8]

Universidade Estadual Paulista, Universidade Federal do ABC, São Paulo, Brazil
C.A. Bernardes[7], F. Damas, T.R. Fernandez Perez Tomei, E.M. Gregores, B. Lopes Da Costa, I. Maietto Silverio, P.G. Mercadante, S.F. Novaes, B. Orzari, Sandra S. Padula, V. Scheurer

Institute for Nuclear Research and Nuclear Energy, Bulgarian Academy of Sciences, Sofia, Bulgaria
A. Aleksandrov, G. Antchev, P. Danev, R. Hadjiiska, P. Iaydjiev, M. Shopova, G. Sultanov

University of Sofia, Sofia, Bulgaria
A. Dimitrov, L. Litov, B. Pavlov, P. Petkov, A. Petrov

Instituto De Alta Investigación, Universidad de Tarapacá, Casilla 7 D, Arica, Chile
S. Keshri, D. Laroze, S. Thakur

Universidad Tecnica Federico Santa Maria, Valparaiso, Chile
W. Brooks

Beihang University, Beijing
T. Cheng, T. Javaid, L. Wang, L. Yuan

Department of Physics, Tsinghua University, Beijing
Z. Hu, Z. Liang, J. Liu, X. Wang, H. Yang

Institute of High Energy Physics, Beijing
G.M. Chen[9], H.S. Chen[9], M. Chen[9], Y. Chen, Q. Hou, X. Hou, F. Iemmi, C.H. Jiang, A. Kapoor[10], H. Liao, G. Liu, Z.-A. Liu[11], J.N. Song[11], S. Song, J. Tao, C. Wang[9], J. Wang, H. Zhang, J. Zhao

State Key Laboratory of Nuclear Physics and Technology, Peking University, Beijing
A. Agapitos, Y. Ban, A. Carvalho Antunes De Oliveira, S. Deng, D. Fu, B. Guo, Q. Guo, C. Jiang, A. Levin, C. Li, Q. Li, Y. Mao, S. Qian, S.J. Qian, X. Qin, C. Quaranta, X. Sun, D. Wang, J. Wang, M. Zhang, Y. Zhao, C. Zhou

State Key Laboratory of Nuclear Physics and Technology, Institute of Quantum Matter, South China Normal University, Guangzhou
S. Yang

Sun Yat-Sen University, Guangzhou
Z. You

University of Science and Technology of China, Hefei
K. Jaffel, N. Lu

Nanjing Normal University, Nanjing
G. Bauer[12,13], Z. Cui[13], B. Li[14], H. Wang, K. Yi[15], J. Zhang

Institute of Modern Physics and Key Laboratory of Nuclear Physics and Ion-beam Application (MOE) - Fudan University, Shanghai
Y. Li

Zhejiang University, Hangzhou, Zhejiang
Z. Lin, C. Lu, M. Xiao[16]

Universidad de Los Andes, Bogota, Colombia
C. Avila, D.A. Barbosa Trujillo, A. Cabrera, C. Florez, J. Fraga, J.A. Reyes Vega

Universidad de Antioquia, Medellin, Colombia
C. Rendón, M. Rodriguez, A.A. Ruales Barbosa, J.D. Ruiz Alvarez

University of Split, Faculty of Electrical Engineering, Mechanical Engineering and Naval Architecture, Split, Croatia
N. Godinovic, D. Lelas, A. Sculac

University of Split, Faculty of Science, Split, Croatia
M. Kovac, A. Petkovic, T. Sculac

Institute Rudjer Boskovic, Zagreb, Croatia
P. Bargassa, V. Brigljevic, B.K. Chitroda, D. Ferencek, K. Jakovcic, A. Starodumov, T. Susa

University of Cyprus, Nicosia, Cyprus
A. Attikis, K. Christoforou, C. Leonidou, C. Nicolaou, L. Paizanos, F. Ptochos, P.A. Razis, H. Rykaczewski, H. Saka, A. Stepennov

Charles University, Prague, Czech Republic
M. Finger[†], M. Finger Jr.

Escuela Politecnica Nacional, Quito, Ecuador
E. Ayala

Universidad San Francisco de Quito, Quito, Ecuador
E. Carrera Jarrin

Academy of Scientific Research and Technology of the Arab Republic of Egypt, Egyptian Network of High Energy Physics, Cairo, Egypt
A.A. Abdelalim[17,18], R. Aly[19,17]

Center for High Energy Physics (CHEP-FU), Fayoum University, El-Fayoum, Egypt
A. Hussein, H. Mohammed

National Institute of Chemical Physics and Biophysics, Tallinn, Estonia
K. Ehataht, M. Kadastik, T. Lange, C. Nielsen, J. Pata, M. Raidal, N. Seeba, L. Tani

Department of Physics, University of Helsinki, Helsinki, Finland
E. Brücken, A. Milieva, K. Osterberg, M. Voutilainen

Helsinki Institute of Physics, Helsinki, Finland
F. Garcia, P. Inkaew, K.T.S. Kallonen, R. Kumar Verma, T. Lampén, K. Lassila-Perini, B. Lehtela, S. Lehti, T. Lindén, N.R. Mancilla Xinto, M. Myllymäki, M.m. Rantanen, S. Saariokari, N.T. Toikka, J. Tuominiemi

Lappeenranta-Lahti University of Technology, Lappeenranta, Finland
N. Bin Norjoharuddeen, H. Kirschenmann, P. Luukka, H. Petrow

IRFU, CEA, Université Paris-Saclay, Gif-sur-Yvette, France
M. Besancon, F. Couderc, M. Dejardin, D. Denegri, P. Devouge, J.L. Faure, F. Ferri, P. Gaigne, S. Ganjour, P. Gras, G. Hamel de Monchenault, M. Kumar, V. Lohezic, Y. Maidannyk, J. Malcles, F. Orlandi, L. Portales, S. Ronchi, M.Ö. Sahin, A. Savoy-Navarro[20], P. Simkina, M. Titov, M. Tornago

Laboratoire Leprince-Ringuet, CNRS/IN2P3, Ecole Polytechnique, Institut Polytechnique de Paris, Palaiseau, France
R. Amella Ranz, F. Beaudette, G. Boldrini, P. Busson, C. Charlot, M. Chiusi, T.D. Cuisset, O. Davignon, A. De Wit, T. Debnath, I.T. Ehle, S. Ghosh, A. Gilbert, R. Granier de Cassagnac, L. Kalipoliti, M. Manoni, M. Nguyen, S. Obraztsov, C. Ochando, R. Salerno, J.B. Sauvan, Y. Sirois, G. Sokmen, L. Urda Gómez, A. Zabi, A. Zghiche

Université de Strasbourg, CNRS, IPHC UMR 7178, Strasbourg, France
J.-L. Agram[21], J. Andrea, D. Bloch, J.-M. Brom, E.C. Chabert, C. Collard, G. Coulon, S. Falke, U. Goerlach, R. Haeberle, A.-C. Le Bihan, M. Meena,

O. Poncet, G. Saha, P. Vaucelle

Centre de Calcul de l'Institut National de Physique Nucleaire et de Physique des Particules, CNRS/IN2P3, Villeurbanne, France
A. Di Florio

Institut de Physique des 2 Infinis de Lyon (IP2I), Villeurbanne, France
D. Amram, S. Beauceron, B. Blancon, G. Boudoul, N. Chanon, D. Contardo, P. Depasse, H. El Mamouni, J. Fay, S. Gascon, M. Gouzevitch, C. Greenberg, G. Grenier, B. Ille, E. Jourd'Huy, M. Lethuillier, B. Massoteau, L. Mirabito, A. Purohit, M. Vander Donckt, J. Xiao

Georgian Technical University, Tbilisi, Georgia
D. Chokheli, I. Lomidze, Z. Tsamalaidze[22]

RWTH Aachen University, I. Physikalisches Institut, Aachen, Germany
V. Botta, S. Consuegra Rodríguez, L. Feld, K. Klein, M. Lipinski, D. Meuser, P. Nattland, V. Oppenländer, A. Pauls, D. Pérez Adán, N. Röwert, M. Teroerde

RWTH Aachen University, III. Physikalisches Institut A, Aachen, Germany
C. Daumann, S. Diekmann, A. Dodonova, N. Eich, D. Eliseev, F. Engelke, J. Erdmann, M. Erdmann, B. Fischer, T. Hebbeker, K. Hoepfner, F. Ivone, A. Jung, N. Kumar, M.y. Lee, F. Mausolf, M. Merschmeyer, A. Meyer, F. Nowotny, A. Pozdnyakov, W. Redjeb, H. Reithler, U. Sarkar, V. Sarkisovi, A. Schmidt, C. Seth, A. Sharma, J.L. Spah, V. Vaulin, S. Zaleski

RWTH Aachen University, III. Physikalisches Institut B, Aachen, Germany
M.R. Beckers, C. Dziwok, G. Flügge, N. Hoeflich, T. Kress, A. Nowack, O. Pooth, A. Stahl, A. Zotz

Deutsches Elektronen-Synchrotron, Hamburg, Germany
H. Aarup Petersen, A. Abel, M. Aldaya Martin, J. Alimena, S. Amoroso, Y. An, I. Andreev, J. Bach, S. Baxter, M. Bayatmakou, H. Becerril Gonzalez, O. Behnke, A. Belvedere, F. Blekman[23], K. Borras[24], A. Campbell, S. Chatterjee, L.X. Coll Saravia, G. Eckerlin, D. Eckstein, E. Gallo[23], A. Geiser, V. Guglielmi, M. Guthoff, A. Hinzmann, L. Jeppe, M. Kasemann, C. Kleinwort, R. Kogler, M. Komm, D. Krücker, W. Lange, D. Leyva Pernia, K.-Y. Lin, K. Lipka[25], W. Lohmann[26], J. Malvaso, R. Mankel, I.-A. Melzer-Pellmann, M. Mendizabal Morentin, A.B. Meyer, G. Milella, K. Moral Figueroa, A. Mussgiller, L.P. Nair, J. Niedziela, A. Nürnberg, J. Park, E. Ranken, A. Raspereza, D. Rastorguev, L. Rygaard, M. Scham[27,24], S. Schnake[24], P. Schütze, C. Schwanenberger[23], D. Selivanova, K. Sharko, M. Shchedrolosiev, D. Stafford, M. Torkian, F. Vazzoler, A. Ventura Barroso, R. Walsh, D. Wang, Q. Wang, K. Wichmann, L. Wiens[24], C. Wissing, Y. Yang, S. Zakharov, A. Zimermmane Castro Santos

University of Hamburg, Hamburg, Germany
A.R. Alves Andrade, M. Antonello, S. Bollweg, M. Bonanomi, K. El Morabit, Y. Fischer, M. Frahm, E. Garutti, A. Grohsjean, A.A. Guvenli, J. Haller, D. Hundhausen, G. Kasieczka, P. Keicher, R. Klanner, W. Korcari, T. Kramer, C.c. Kuo, F. Labe, J. Lange, A. Lobanov, L. Moureaux, A. Nigamova, K. Nikolopoulos, A. Paasch, K.J. Pena Rodriguez, N. Prouvost, B. Raciti, M. Rieger, D. Savoiu, P. Schleper, M. Schröder, J. Schwandt, M. Sommerhalder, H. Stadie,

G. Steinbrück, R. Ward, B. Wiederspan, M. Wolf

Karlsruher Institut fuer Technologie, Karlsruhe, Germany
S. Brommer, E. Butz, Y.M. Chen, T. Chwalek, A. Dierlamm, G.G. Dincer, U. Elicabuk, N. Faltermann, M. Giffels, A. Gottmann, F. Hartmann[28], M. Horzela, F. Hummer, U. Husemann, J. Kieseler, M. Klute, R. Kunnilan Muhammed Rafeek, O. Lavoryk, J.M. Lawhorn, A. Lintuluoto, S. Maier, M. Mormile, Th. Müller, E. Pfeffer, M. Presilla, G. Quast, K. Rabbertz, B. Regnery, R. Schmieder, N. Shadskiy, I. Shvetsov, H.J. Simonis, L. Sowa, L. Stockmeier, K. Tauqeer, M. Toms, B. Topko, N. Trevisani, C. Verstege, T. Voigtländer, R.F. Von Cube, J. Von Den Driesch, M. Wassmer, R. Wolf, W.D. Zeuner, X. Zuo

Institute of Nuclear and Particle Physics (INPP), NCSR Demokritos, Aghia Paraskevi, Greece
G. Anagnostou, G. Daskalakis, A. Kyriakis

National and Kapodistrian University of Athens, Athens, Greece
G. Melachroinos, Z. Painesis, I. Paraskevas, N. Saoulidou, K. Theofilatos, E. Tziaferi, E. Tzovara, K. Vellidis, I. Zisopoulos

National Technical University of Athens, Athens, Greece
T. Chatzistavrou, G. Karapostoli, K. Kousouris, E. Siamarkou, G. Tsipolitis

University of Ioánnina, Ioánnina, Greece
I. Bestintzanos, I. Evangelou, C. Foudas, P. Katsoulis, P. Kokkas, P.G. Kosmoglou Kioseoglou, N. Manthos, I. Papadopoulos, J. Strologas

HUN-REN Wigner Research Centre for Physics, Budapest, Hungary
D. Druzhkin, C. Hajdu, D. Horvath[29,30], K. Márton, A.J. Rádl[31], F. Sikler, V. Veszpremi

MTA-ELTE Lendület CMS Particle and Nuclear Physics Group, Eötvös Loránd University, Budapest, Hungary
M. Csanád, K. Farkas, A. Fehérkuti[32], M.M.A. Gadallah[33], Á. Kadlecsik, M. León Coello, G. Pásztor, G.I. Veres

Faculty of Informatics, University of Debrecen, Debrecen, Hungary
B. Ujvari, G. Zilizi

HUN-REN ATOMKI - Institute of Nuclear Research, Debrecen, Hungary
G. Bencze, S. Czellar, J. Molnar, Z. Szillasi

Karoly Robert Campus, MATE Institute of Technology, Gyongyos, Hungary
T. Csorgo[32], F. Nemes[32], T. Novak, I. Szanyi[34]

Panjab University, Chandigarh, India
S. Bansal, S.B. Beri, V. Bhatnagar, G. Chaudhary, S. Chauhan, N. Dhingra[35], A. Kaur, A. Kaur, H. Kaur, M. Kaur, S. Kumar, T. Sheokand, J.B. Singh, A. Singla

University of Delhi, Delhi, India
A. Bhardwaj, A. Chhetri, B.C. Choudhary, A. Kumar, A. Kumar, M. Naimuddin, S. Phor, K. Ranjan, M.K. Saini

University of Hyderabad, Hyderabad, India
S. Acharya[36], B. Gomber, B. Sahu[36]

Indian Institute of Technology Kanpur, Kanpur, India
S. Mukherjee

Saha Institute of Nuclear Physics, HBNI, Kolkata, India
S. Baradia, S. Bhattacharya, S. Das Gupta, S. Dutta, S. Dutta, S. Sarkar

Indian Institute of Technology Madras, Madras, India
M.M. Ameen, P.K. Behera, S. Chatterjee, G. Dash, A. Dattamunsi, P. Jana, P. Kalbhor, S. Kamble, J.R. Komaragiri[37], T. Mishra, P.R. Pujahari, A.K. Sikdar, R.K. Singh, P. Verma, S. Verma, A. Vijay

IISER Mohali, India, Mohali, India
B.K. Sirasva

Tata Institute of Fundamental Research-A, Mumbai, India
L. Bhatt, S. Dugad, G.B. Mohanty, M. Shelake, P. Suryadevara

Tata Institute of Fundamental Research-B, Mumbai, India
A. Bala, S. Banerjee, S. Barman[38], R.M. Chatterjee, M. Guchait, Sh. Jain, A. Jaiswal, B.M. Joshi, S. Kumar, M. Maity[38], G. Majumder, K. Mazumdar, S. Parolia, R. Saxena, A. Thachayath

National Institute of Science Education and Research, An OCC of Homi Bhabha National Institute, Bhubaneswar, Odisha, India
S. Bahinipati[39], D. Maity[40], P. Mal, K. Naskar[40], A. Nayak[40], S. Nayak, K. Pal, R. Raturi, P. Sadangi, S.K. Swain, S. Varghese[40], D. Vats[40]

Indian Institute of Science Education and Research (IISER), Pune, India
A. Alpana, S. Dube, P. Hazarika, B. Kansal, A. Laha, R. Sharma, S. Sharma, K.Y. Vaish

Indian Institute of Technology Hyderabad, Telangana, India
S. Ghosh

Isfahan University of Technology, Isfahan, Iran
H. Bakhshiansohi[41], A. Jafari[42], V. Sedighzadeh Dalavi, M. Zeinali[43]

Institute for Research in Fundamental Sciences (IPM), Tehran, Iran
S. Bashiri, S. Chenarani[44], S.M. Etesami, Y. Hosseini, M. Khakzad, E. Khazaie, M. Mohammadi Najafabadi, S. Tizchang[45]

University College Dublin, Dublin, Ireland
M. Felcini, M. Grunewald

INFN Sezione di Bari[a], Università di Bari[b], Politecnico di Bari[c], Bari, Italy
M. Abbrescia[a,b], M. Barbieri[a,b], M. Buonsante[a,b], A. Colaleo[a,b], D. Creanza[a,c], N. De Filippis[a,c], M. De Palma[a,b], W. Elmetenawee[a,b,17], N. Ferrara[a,c], L. Fiore[a], L. Longo[a], M. Louka[a,b], G. Maggi[a,c], M. Maggi[a], I. Margjeka[a], V. Mastrapasqua[a,b], S. My[a,b], F. Nenna[a,b], S. Nuzzo[a,b], A. Pellecchia[a,b], A. Pompili[a,b], G. Pugliese[a,c], R. Radogna[a,b], D. Ramos[a], A. Ranieri[a], L. Silvestris[a], F.M. Simone[a,c], Ü. Sözbilir[a], A. Stamerra[a,b], D. Troiano[a,b], R. Venditti[a,b], P. Verwilligen[a], A. Zaza[a,b]

INFN Sezione di Bologna[a], Università di Bologna[b], Bologna, Italy
G. Abbiendi[a], C. Battilana[a,b], D. Bonacorsi[a,b], P. Capiluppi[a,b], F.R. Cavallo[a], M. Cuffiani[a,b], G.M. Dallavalle[a], T. Diotalevi[a,b], F. Fabbri[a], A. Fanfani[a,b],

R. Farinelli[a], D. Fasanella[a], P. Giacomelli[a], C. Grandi[a], L. Guiducci[a,b], M. Lorusso[a,b], L. Lunerti[a], G. Masetti[a], F.L. Navarria[a,b], G. Paggi[a,b], A. Perrotta[a], F. Primavera[a,b], A.M. Rossi[a,b], S. Rossi Tisbeni[a,b], T. Rovelli[a,b], G.P. Siroli[a,b]

INFN Sezione di Catania[a], Università di Catania[b], Catania, Italy
S. Costa[a,b,46], A. Di Mattia[a], A. Lapertosa[a], R. Potenza[a,b], A. Tricomi[a,b,46]

INFN Sezione di Firenze[a], Università di Firenze[b], Firenze, Italy
J. Altork[a,b], P. Assiouras[a], G. Barbagli[a], G. Bardelli[a], M. Bartolini[a,b], A. Calandri[a,b], B. Camaiani[a,b], A. Cassese[a], R. Ceccarelli[a], V. Ciulli[a,b], C. Civinini[a], R. D'Alessandro[a,b], L. Damenti[a,b], E. Focardi[a,b], T. Kello[a], G. Latino[a,b], P. Lenzi[a,b], M. Lizzo[a], M. Meschini[a], S. Paoletti[a], A. Papanastassiou[a,b], G. Sguazzoni[a], L. Viliani[a]

INFN Laboratori Nazionali di Frascati, Frascati, Italy
L. Benussi, S. Bianco, S. Meola[47], D. Piccolo

INFN Sezione di Genova[a], Università di Genova[b], Genova, Italy
M. Alves Gallo Pereira[a], F. Ferro[a], E. Robutti[a], S. Tosi[a,b]

INFN Sezione di Milano-Bicocca[a], Università di Milano-Bicocca[b], Milano, Italy
A. Benaglia[a], F. Brivio[a], V. Camagni[a,b], F. Cetorelli[a,b], F. De Guio[a,b], M.E. Dinardo[a,b], P. Dini[a], S. Gennai[a], R. Gerosa[a,b], A. Ghezzi[a,b], P. Govoni[a,b], L. Guzzi[a], M.R. Kim[a], G. Lavizzari[a,b], M.T. Lucchini[a,b], M. Malberti[a], S. Malvezzi[a], A. Massironi[a], D. Menasce[a], L. Moroni[a], M. Paganoni[a,b], S. Palluotto[a,b], D. Pedrini[a], A. Perego[a,b], G. Pizzati[a,b], S. Ragazzi[a,b], T. Tabarelli de Fatis[a,b]

INFN Sezione di Napoli[a], Università di Napoli 'Federico II'[b], Napoli, Italy; Università della Basilicata[c], Potenza, Italy; Scuola Superiore Meridionale (SSM)[d], Napoli, Italy
S. Buontempo[a], C. Di Fraia[a,b], F. Fabozzi[a,c], L. Favilla[a,d], A.O.M. Iorio[a,b], L. Lista[a,b,48], P. Paolucci[a,28], B. Rossi[a]

INFN Sezione di Padova[a], Università di Padova[b], Padova, Italy; Universita degli Studi di Cagliari[c], Cagliari, Italy
P. Azzi[a], N. Bacchetta[a,49], D. Bisello[a,b], P. Bortignon[a,c], G. Bortolato[a,b], A.C.M. Bulla[a,c], P. Checchia[a], T. Dorigo[a,50], F. Gasparini[a,b], U. Gasparini[a,b], S. Giorgetti[a], E. Lusiani[a], M. Margoni[a,b], A.T. Meneguzzo[a,b], J. Pazzini[a,b], P. Ronchese[a,b], R. Rossin[a,b], M. Sgaravatto[a], F. Simonetto[a,b], M. Tosi[a,b], A. Triossi[a,b], S. Ventura[a], M. Zanetti[a,b], P. Zotto[a,b], A. Zucchetta[a,b]

INFN Sezione di Pavia[a], Università di Pavia[b], Pavia, Italy
A. Braghieri[a], S. Calzaferri[a], P. Montagna[a,b], M. Pelliccioni[a], V. Re[a], C. Riccardi[a,b], P. Salvini[a], I. Vai[a,b], P. Vitulo[a,b]

INFN Sezione di Perugia[a], Università di Perugia[b], Perugia, Italy
S. Ajmal[a,b], M.E. Ascioti[a,b], G.M. Bilei[a], C. Carrivale[a,b], D. Ciangottini[a,b], L. Della Penna[a,b], L. Fanò[a,b], V. Mariani[a,b], M. Menichelli[a], F. Moscatelli[a,51], A. Rossi[a,b], A. Santocchia[a,b], D. Spiga[a], T. Tedeschi[a,b]

INFN Sezione di Pisa[a], Università di Pisa[b], Scuola Normale Superiore di Pisa[c], Pisa, Italy; Università di Siena[d], Siena, Italy
C. Aimè[a,b], C.A. Alexe[a,c], P. Asenov[a,b], P. Azzurri[a], G. Bagliesi[a], L. Bianchini[a,b],

T. Boccali[a], E. Bossini[a], D. Bruschini[a,c], L. Calligaris[a,b], R. Castaldi[a], F. Cattafesta[a,c], M.A. Ciocci[a,d], M. Cipriani[a,b], R. Dell'Orso[a], S. Donato[a,b], R. Forti[a,b], A. Giassi[a], F. Ligabue[a,c], A.C. Marini[a,b], D. Matos Figueiredo[a], A. Messineo[a,b], S. Mishra[a], V.K. Muraleedharan Nair Bindhu[a,b], S. Nandan[a], F. Palla[a], M. Riggirello[a,c], A. Rizzi[a,b], G. Rolandi[a,c], S. Roy Chowdhury[a,52], T. Sarkar[a], A. Scribano[a], P. Solanki[a,b], P. Spagnolo[a], F. Tenchini[a,b], R. Tenchini[a], G. Tonelli[a,b], N. Turini[a,d], F. Vaselli[a,c], A. Venturi[a], P.G. Verdini[a]

INFN Sezione di Roma[a], Sapienza Università di Roma[b], Roma, Italy
P. Akrap[a,b], C. Basile[a,b], S.C. Behera[a], F. Cavallari[a], L. Cunqueiro Mendez[a,b], F. De Riggi[a,b], D. Del Re[a,b], E. Di Marco[a], M. Diemoz[a], F. Errico[a], L. Frosina[a,b], R. Gargiulo[a,b], B. Harikrishnan[a,b], F. Lombardi[a,b], E. Longo[a,b], L. Martikainen[a,b], J. Mijuskovic[a,b], G. Organtini[a,b], N. Palmeri[a,b], R. Paramatti[a,b], S. Rahatlou[a,b], C. Rovelli[a], F. Santanastasio[a,b], L. Soffi[a], V. Vladimirov[a,b]

INFN Sezione di Torino[a], Università di Torino[b], Torino, Italy; Università del Piemonte Orientale[c], Novara, Italy
N. Amapane[a,b], R. Arcidiacono[a,c], S. Argiro[a,b], M. Arneodo[a,c], N. Bartosik[a,c], R. Bellan[a,b], A. Bellora[a,b], C. Biino[a], C. Borca[a,b], N. Cartiglia[a], M. Costa[a,b], R. Covarelli[a,b], N. Demaria[a], L. Finco[a], M. Grippo[a,b], B. Kiani[a,b], L. Lanteri[a,b], F. Legger[a], F. Luongo[a,b], C. Mariotti[a], S. Maselli[a], A. Mecca[a,b], L. Menzio[a,b], P. Meridiani[a], E. Migliore[a,b], M. Monteno[a], M.M. Obertino[a,b], G. Ortona[a], L. Pacher[a,b], N. Pastrone[a], M. Ruspa[a,c], F. Siviero[a,b], V. Sola[a,b], A. Solano[a,b], A. Staiano[a], C. Tarricone[a,b], D. Trocino[a], G. Umoret[a,b], E. Vlasov[a,b], R. White[a,b]

INFN Sezione di Trieste[a], Università di Trieste[b], Trieste, Italy
J. Babbar[a,b], S. Belforte[a], V. Candelise[a,b], M. Casarsa[a], F. Cossutti[a], K. De Leo[a], G. Della Ricca[a,b], R. Delli Gatti[a,b]

Kyungpook National University, Daegu, Korea
S. Dogra, J. Hong, J. Kim, T. Kim, D. Lee, H. Lee, J. Lee, S.W. Lee, C.S. Moon, Y.D. Oh, S. Sekmen, B. Tae, Y.C. Yang

Department of Mathematics and Physics - GWNU, Gangneung, Korea
M.S. Kim

Chonnam National University, Institute for Universe and Elementary Particles, Kwangju, Korea
G. Bak, P. Gwak, H. Kim, D.H. Moon, J. Seo

Hanyang University, Seoul, Korea
E. Asilar, F. Carnevali, J. Choi[53], T.J. Kim, Y. Ryou

Korea University, Seoul, Korea
S. Ha, S. Han, B. Hong, J. Kim, K. Lee, K.S. Lee, S. Lee, J. Yoo

Kyung Hee University, Department of Physics, Seoul, Korea
J. Goh, J. Shin, S. Yang

Sejong University, Seoul, Korea
Y. Kang, H. S. Kim, Y. Kim, S. Lee

Seoul National University, Seoul, Korea
J. Almond, J.H. Bhyun, J. Choi, J. Choi, W. Jun, H. Kim, J. Kim, T. Kim, Y. Kim, Y.W. Kim, S. Ko, H. Lee, J. Lee, J. Lee, B.H. Oh, S.B. Oh, J. Shin, U.K. Yang,

I. Yoon

University of Seoul, Seoul, Korea
W. Jang, D.Y. Kang, D. Kim, S. Kim, B. Ko, J.S.H. Lee, Y. Lee, I.C. Park, Y. Roh, I.J. Watson

Yonsei University, Department of Physics, Seoul, Korea
G. Cho, K. Hwang, B. Kim, S. Kim, K. Lee, H.D. Yoo

Sungkyunkwan University, Suwon, Korea
Y. Lee, I. Yu

College of Engineering and Technology, American University of the Middle East (AUM), Dasman, Kuwait
T. Beyrouthy, Y. Gharbia

Kuwait University - College of Science - Department of Physics, Safat, Kuwait
F. Alazemi

Riga Technical University, Riga, Latvia
K. Dreimanis, O.M. Eberlins, A. Gaile, C. Munoz Diaz, D. Osite, G. Pikurs, R. Plese, A. Potrebko, M. Seidel, D. Sidiropoulos Kontos

University of Latvia (LU), Riga, Latvia
N.R. Strautnieks

Vilnius University, Vilnius, Lithuania
M. Ambrozas, A. Juodagalvis, S. Nargelas, A. Rinkevicius, G. Tamulaitis

National Centre for Particle Physics, Universiti Malaya, Kuala Lumpur, Malaysia
I. Yusuff[54], Z. Zolkapli

Universidad de Sonora (UNISON), Hermosillo, Mexico
J.F. Benitez, A. Castaneda Hernandez, A. Cota Rodriguez, L.E. Cuevas Picos, H.A. Encinas Acosta, L.G. Gallegos Maríñez, J.A. Murillo Quijada, L. Valencia Palomo

Centro de Investigacion y de Estudios Avanzados del IPN, Mexico City, Mexico
G. Ayala, H. Castilla-Valdez, H. Crotte Ledesma, R. Lopez-Fernandez, J. Mejia Guisao, R. Reyes-Almanza, A. Sánchez Hernández

Universidad Iberoamericana, Mexico City, Mexico
C. Oropeza Barrera, D.L. Ramirez Guadarrama, M. Ramírez García

Benemerita Universidad Autonoma de Puebla, Puebla, Mexico
I. Bautista, F.E. Neri Huerta, I. Pedraza, H.A. Salazar Ibarguen, C. Uribe Estrada

University of Montenegro, Podgorica, Montenegro
I. Bubanja, N. Raicevic

University of Canterbury, Christchurch, New Zealand
P.H. Butler

National Centre for Physics, Quaid-I-Azam University, Islamabad, Pakistan
A. Ahmad, M.I. Asghar, A. Awais, M.I.M. Awan, W.A. Khan

AGH University of Krakow, Krakow, Poland
V. Avati, L. Forthomme, L. Grzanka, M. Malawski, K. Piotrzkowski

National Centre for Nuclear Research, Swierk, Poland
M. Bluj, M. Górski, M. Kazana, M. Szleper, P. Zalewski

Institute of Experimental Physics, Faculty of Physics, University of Warsaw, Warsaw, Poland
K. Bunkowski, K. Doroba, A. Kalinowski, M. Konecki, J. Krolikowski, A. Muhammad

Warsaw University of Technology, Warsaw, Poland
P. Fokow, K. Pozniak, W. Zabolotny

Laboratório de Instrumentação e Física Experimental de Partículas, Lisboa, Portugal
M. Araujo, D. Bastos, C. Beirão Da Cruz E Silva, A. Boletti, M. Bozzo, T. Camporesi, G. Da Molin, M. Gallinaro, J. Hollar, N. Leonardo, G.B. Marozzo, A. Petrilli, M. Pisano, J. Seixas, J. Varela, J.W. Wulff

Faculty of Physics, University of Belgrade, Belgrade, Serbia
P. Adzic, L. Markovic, P. Milenovic, V. Milosevic

VINCA Institute of Nuclear Sciences, University of Belgrade, Belgrade, Serbia
D. Devetak, M. Dordevic, J. Milosevic, L. Nadderd, V. Rekovic, M. Stojanovic

Centro de Investigaciones Energéticas Medioambientales y Tecnológicas (CIEMAT), Madrid, Spain
M. Alcalde Martinez, J. Alcaraz Maestre, Cristina F. Bedoya, J.A. Brochero Cifuentes, Oliver M. Carretero, M. Cepeda, M. Cerrada, N. Colino, B. De La Cruz, A. Delgado Peris, A. Escalante Del Valle, D. Fernández Del Val, J.P. Fernández Ramos, J. Flix, M.C. Fouz, M. Gonzalez Hernandez, O. Gonzalez Lopez, S. Goy Lopez, J.M. Hernandez, M.I. Josa, J. Llorente Merino, C. Martin Perez, E. Martin Viscasillas, D. Moran, C. M. Morcillo Perez, Á. Navarro Tobar, R. Paz Herrera, C. Perez Dengra, A. Pérez-Calero Yzquierdo, J. Puerta Pelayo, I. Redondo, J. Vazquez Escobar

Universidad Autónoma de Madrid, Madrid, Spain
J.F. de Trocóniz

Universidad de Oviedo, Instituto Universitario de Ciencias y Tecnologías Espaciales de Asturias (ICTEA), Oviedo, Spain
B. Alvarez Gonzalez, J. Ayllon Torresano, A. Cardini, J. Cuevas, J. Del Riego Badas, D. Estrada Acevedo, J. Fernandez Menendez, S. Folgueras, I. Gonzalez Caballero, P. Leguina, M. Obeso Menendez, E. Palencia Cortezon, J. Prado Pico, A. Soto Rodríguez, C. Vico Villalba, P. Vischia

Instituto de Física de Cantabria (IFCA), CSIC-Universidad de Cantabria, Santander, Spain
S. Blanco Fernández, I.J. Cabrillo, A. Calderon, J. Duarte Campderros, M. Fernandez, G. Gomez, C. Lasaosa García, R. Lopez Ruiz, C. Martinez Rivero, P. Martinez Ruiz del Arbol, F. Matorras, P. Matorras Cuevas, E. Navarrete Ramos, J. Piedra Gomez, C. Quintana San Emeterio, L. Scodellaro, I. Vila, R. Vilar Cortabitarte, J.M. Vizan Garcia

University of Colombo, Colombo, Sri Lanka
B. Kailasapathy[55], D.D.C. Wickramarathna

University of Ruhuna, Department of Physics, Matara, Sri Lanka
W.G.D. Dharmaratna[56], K. Liyanage, N. Perera

CERN, European Organization for Nuclear Research, Geneva, Switzerland
D. Abbaneo, C. Amendola, R. Ardino, E. Auffray, J. Baechler, D. Barney, J. Bendavid, M. Bianco, A. Bocci, L. Borgonovi, C. Botta, A. Bragagnolo, C.E. Brown, C. Caillol, G. Cerminara, P. Connor, D. d'Enterria, A. Dabrowski, A. David, A. De Roeck, M.M. Defranchis, M. Deile, M. Dobson, P.J. Fernández Manteca, B.A. Fontana Santos Alves, W. Funk, A. Gaddi, S. Giani, D. Gigi, K. Gill, F. Glege, M. Glowacki, A. Gruber, J. Hegeman, J.K. Heikkilä, R. Hofsaess, B. Huber, T. James, P. Janot, O. Kaluzinska, O. Karacheban[26], G. Karathanasis, S. Laurila, P. Lecoq, E. Leutgeb, C. Lourenço, A.-M. Lyon, M. Magherini, L. Malgeri, M. Mannelli, A. Mehta, F. Meijers, J.A. Merlin, S. Mersi, E. Meschi, M. Migliorini, F. Monti, F. Moortgat, M. Mulders, M. Musich, I. Neutelings, S. Orfanelli, F. Pantaleo, M. Pari, G. Petrucciani, A. Pfeiffer, M. Pierini, M. Pitt, H. Qu, D. Rabady, A. Reimers, B. Ribeiro Lopes, F. Riti, P. Rosado, M. Rovere, H. Sakulin, R. Salvatico, S. Sanchez Cruz, S. Scarfi, M. Selvaggi, A. Sharma, K. Shchelina, P. Silva, P. Sphicas[57], A.G. Stahl Leiton, A. Steen, S. Summers, D. Treille, P. Tropea, E. Vernazza, J. Wanczyk[58], J. Wang, S. Wuchterl, M. Zarucki, P. Zehetner, P. Zejdl, G. Zevi Della Porta

PSI Center for Neutron and Muon Sciences, Villigen, Switzerland
T. Bevilacqua[59], L. Caminada[59], W. Erdmann, R. Horisberger, Q. Ingram, H.C. Kaestli, D. Kotlinski, C. Lange, U. Langenegger, L. Noehte[59], T. Rohe, A. Samalan

ETH Zurich - Institute for Particle Physics and Astrophysics (IPA), Zurich, Switzerland
T.K. Aarrestad, M. Backhaus, G. Bonomelli, C. Cazzaniga, K. Datta, P. De Bryas Dexmiers D'Archiacchiac[58], A. De Cosa, G. Dissertori, M. Dittmar, M. Donegà, F. Eble, K. Gedia, F. Glessgen, C. Grab, N. Härringer, T.G. Harte, W. Lustermann, M. Malucchi, R.A. Manzoni, M. Marchegiani, L. Marchese, A. Mascellani[58], F. Nessi-Tedaldi, F. Pauss, V. Perovic, B. Ristic, R. Seidita, J. Steggemann[58], A. Tarabini, D. Valsecchi, R. Wallny

Universität Zürich, Zurich, Switzerland
C. Amsler[60], P. Bärtschi, F. Bilandzija, M.F. Canelli, G. Celotto, K. Cormier, M. Huwiler, W. Jin, A. Jofrehei, B. Kilminster, T.H. Kwok, S. Leontsinis, V. Lukashenko, A. Macchiolo, F. Meng, M. Missiroli, J. Motta, P. Robmann, M. Senger, E. Shokr, F. Stäger, R. Tramontano, P. Viscone

National Central University, Chung-Li
D. Bhowmik, C.M. Kuo, P.K. Rout, S. Taj, P.C. Tiwari[37]

National Taiwan University (NTU), Taipei
L. Ceard, K.F. Chen, Z.g. Chen, A. De Iorio, W.-S. Hou, T.h. Hsu, Y.w. Kao, S. Karmakar, G. Kole, Y.y. Li, R.-S. Lu, E. Paganis, X.f. Su, J. Thomas-Wilsker, L.s. Tsai, D. Tsionou, H.y. Wu, E. Yazgan

High Energy Physics Research Unit, Department of Physics, Faculty of Science, Chulalongkorn University, Bangkok, Thailand
C. Asawatangtrakuldee, N. Srimanobhas

Tunis El Manar University, Tunis, Tunisia
Y. Maghrbi

Çukurova University, Physics Department, Science and Art Faculty, Adana, Turkey

D. Agyel, F. Dolek, I. Dumanoglu[61], Y. Guler[62], E. Gurpinar Guler[62], C. Isik, O. Kara, A. Kayis Topaksu, Y. Komurcu, G. Onengut, K. Ozdemir[63], B. Tali[64], U.G. Tok, E. Uslan, I.S. Zorbakir

Hacettepe University, Ankara, Turkey
S. Sen

Middle East Technical University, Physics Department, Ankara, Turkey
M. Yalvac[65]

Bogazici University, Istanbul, Turkey
B. Akgun, I.O. Atakisi[66], E. Gülmez, M. Kaya[67], O. Kaya[68], M.A. Sarkisla[69], S. Tekten[70]

Istanbul Technical University, Istanbul, Turkey
A. Cakir, K. Cankocak[61,71]

Istanbul University, Istanbul, Turkey
B. Hacisahinoglu, I. Hos[72], B. Kaynak, S. Ozkorucuklu, O. Potok, H. Sert, C. Simsek, C. Zorbilmez

Yildiz Technical University, Istanbul, Turkey
S. Cerci, C. Dozen[73], B. Isildak[74], E. Simsek, D. Sunar Cerci, T. Yetkin[73]

Institute for Scintillation Materials of National Academy of Science of Ukraine, Kharkiv, Ukraine
A. Boyaryntsev, O. Dadazhanova, B. Grynyov

National Science Centre, Kharkiv Institute of Physics and Technology, Kharkiv, Ukraine
L. Levchuk

University of Bristol, Bristol, United Kingdom
J.J. Brooke, A. Bundock, F. Bury, E. Clement, D. Cussans, D. Dharmender, H. Flacher, J. Goldstein, H.F. Heath, M.-L. Holmberg, L. Kreczko, S. Paramesvaran, L. Robertshaw, M.S. Sanjrani[41], J. Segal, V.J. Smith

Rutherford Appleton Laboratory, Didcot, United Kingdom
A.H. Ball, K.W. Bell, A. Belyaev[75], C. Brew, R.M. Brown, D.J.A. Cockerill, A. Elliot, K.V. Ellis, J. Gajownik, K. Harder, S. Harper, J. Linacre, K. Manolopoulos, M. Moallemi, D.M. Newbold, E. Olaiya, D. Petyt, T. Reis, A.R. Sahasransu, G. Salvi, T. Schuh, C.H. Shepherd-Themistocleous, I.R. Tomalin, K.C. Whalen, T. Williams

Imperial College, London, United Kingdom
I. Andreou, R. Bainbridge, P. Bloch, O. Buchmuller, C.A. Carrillo Montoya, D. Colling, I. Das, P. Dauncey, G. Davies, M. Della Negra, S. Fayer, G. Fedi, G. Hall, H.R. Hoorani, A. Howard, G. Iles, C.R. Knight, P. Krueper, J. Langford, K.H. Law, J. León Holgado, L. Lyons, A.-M. Magnan, B. Maier, S. Mallios, A. Mastronikolis, M. Mieskolainen, J. Nash[76], M. Pesaresi, P.B. Pradeep, B.C. Radburn-Smith, A. Richards, A. Rose, L. Russell, K. Savva, C. Seez, R. Shukla, A. Tapper, K. Uchida, G.P. Uttley, T. Virdee[28], M. Vojinovic, N. Wardle, D. Winterbottom

Brunel University, Uxbridge, United Kingdom
J.E. Cole, A. Khan, P. Kyberd, I.D. Reid

Baylor University, Waco, Texas, USA
S. Abdullin, A. Brinkerhoff, E. Collins, M.R. Darwish, J. Dittmann, K. Hatakeyama, V. Hegde, J. Hiltbrand, B. McMaster, J. Samudio, S. Sawant, C. Sutantawibul, J. Wilson

Bethel University, St. Paul, Minnesota, USA
J.M. Hogan[77]

Catholic University of America, Washington, DC, USA
R. Bartek, A. Dominguez, S. Raj, A.E. Simsek, S.S. Yu

The University of Alabama, Tuscaloosa, Alabama, USA
B. Bam, A. Buchot Perraguin, S. Campbell, R. Chudasama, S.I. Cooper, C. Crovella, G. Fidalgo, S.V. Gleyzer, A. Khukhunaishvili, K. Matchev, E. Pearson, C.U. Perez, P. Rumerio[78], E. Usai, R. Yi

Boston University, Boston, Massachusetts, USA
S. Cholak, G. De Castro, Z. Demiragli, C. Erice, C. Fangmeier, C. Fernandez Madrazo, E. Fontanesi, J. Fulcher, F. Golf, S. Jeon, J. O'Cain, I. Reed, J. Rohlf, K. Salyer, D. Sperka, D. Spitzbart, I. Suarez, A. Tsatsos, E. Wurtz, A.G. Zecchinelli

Brown University, Providence, Rhode Island, USA
G. Barone, G. Benelli, D. Cutts, S. Ellis, L. Gouskos, M. Hadley, U. Heintz, K.W. Ho, T. Kwon, L. Lambrecht, G. Landsberg, K.T. Lau, J. Luo, S. Mondal, J. Roloff, T. Russell, S. Sagir[79], X. Shen, M. Stamenkovic, N. Venkatasubramanian

University of California, Davis, Davis, California, USA
S. Abbott, B. Barton, R. Breedon, H. Cai, M. Calderon De La Barca Sanchez, E. Cannaert, M. Chertok, M. Citron, J. Conway, P.T. Cox, R. Erbacher, O. Kukral, G. Mocellin, S. Ostrom, I. Salazar Segovia, J.S. Tafoya Vargas, W. Wei, S. Yoo

University of California, Los Angeles, California, USA
K. Adamidis, M. Bachtis, D. Campos, R. Cousins, A. Datta, G. Flores Avila, J. Hauser, M. Ignatenko, M.A. Iqbal, T. Lam, Y.f. Lo, E. Manca, A. Nunez Del Prado, D. Saltzberg, V. Valuev

University of California, Riverside, Riverside, California, USA
R. Clare, J.W. Gary, G. Hanson

University of California, San Diego, La Jolla, California, USA
A. Aportela, A. Arora, J.G. Branson, S. Cittolin, S. Cooperstein, B. D'Anzi, D. Diaz, J. Duarte, L. Giannini, Y. Gu, J. Guiang, V. Krutelyov, R. Lee, J. Letts, H. Li, M. Masciovecchio, F. Mokhtar, S. Mukherjee, M. Pieri, D. Primosch, M. Quinnan, V. Sharma, M. Tadel, E. Vourliotis, F. Würthwein, A. Yagil, Z. Zhao

University of California, Santa Barbara - Department of Physics, Santa Barbara, California, USA
A. Barzdukas, L. Brennan, C. Campagnari, S. Carron Montero[80], K. Downham, C. Grieco, M.M. Hussain, J. Incandela, M.W.K. Lai, A.J. Li, P. Masterson, J. Richman, S.N. Santpur, U. Sarica, R. Schmitz, F. Setti, J. Sheplock, D. Stuart, T.Á. Vámi, X. Yan, D. Zhang

California Institute of Technology, Pasadena, California, USA

A. Albert, S. Bhattacharya, A. Bornheim, O. Cerri, R. Kansal, J. Mao, H.B. Newman, G. Reales Gutiérrez, T. Sievert, M. Spiropulu, J.R. Vlimant, R.A. Wynne, S. Xie

Carnegie Mellon University, Pittsburgh, Pennsylvania, USA
J. Alison, S. An, M. Cremonesi, V. Dutta, E.Y. Ertorer, T. Ferguson, T.A. Gómez Espinosa, A. Harilal, A. Kallil Tharayil, M. Kanemura, C. Liu, P. Meiring, T. Mudholkar, S. Murthy, P. Palit, K. Park, M. Paulini, A. Roberts, A. Sanchez, W. Terrill

University of Colorado Boulder, Boulder, Colorado, USA
J.P. Cumalat, W.T. Ford, A. Hart, S. Kwan, J. Pearkes, C. Savard, N. Schonbeck, K. Stenson, K.A. Ulmer, S.R. Wagner, N. Zipper, D. Zuolo

Cornell University, Ithaca, New York, USA
J. Alexander, X. Chen, J. Dickinson, A. Duquette, J. Fan, X. Fan, J. Grassi, S. Hogan, P. Kotamnives, J. Monroy, G. Niendorf, M. Oshiro, J.R. Patterson, A. Ryd, J. Thom, P. Wittich, R. Zou, L. Zygala

Fermi National Accelerator Laboratory, Batavia, Illinois, USA
M. Albrow, M. Alyari, O. Amram, G. Apollinari, A. Apresyan, L.A.T. Bauerdick, D. Berry, J. Berryhill, P.C. Bhat, K. Burkett, J.N. Butler, A. Canepa, G.B. Cerati, H.W.K. Cheung, F. Chlebana, C. Cosby, G. Cummings, I. Dutta, V.D. Elvira, J. Freeman, A. Gandrakota, Z. Gecse, L. Gray, D. Green, A. Grummer, S. Grünendahl, D. Guerrero, O. Gutsche, R.M. Harris, T.C. Herwig, J. Hirschauer, V. Innocente, B. Jayatilaka, S. Jindariani, M. Johnson, U. Joshi, B. Klima, K.H.M. Kwok, S. Lammel, C. Lee, D. Lincoln, R. Lipton, T. Liu, K. Maeshima, D. Mason, P. McBride, P. Merkel, S. Mrenna, S. Nahn, J. Ngadiuba, D. Noonan, S. Norberg, V. Papadimitriou, N. Pastika, K. Pedro, C. Pena[81], C.E. Perez Lara, F. Ravera, A. Reinsvold Hall[82], L. Ristori, M. Safdari, E. Sexton-Kennedy, N. Smith, A. Soha, L. Spiegel, S. Stoynev, J. Strait, L. Taylor, S. Tkaczyk, N.V. Tran, L. Uplegger, E.W. Vaandering, C. Wang, I. Zoi

University of Florida, Gainesville, Florida, USA
C. Aruta, P. Avery, D. Bourilkov, P. Chang, V. Cherepanov, R.D. Field, C. Huh, E. Koenig, M. Kolosova, J. Konigsberg, A. Korytov, G. Mitselmakher, K. Mohrman, A. Muthirakalayil Madhu, N. Rawal, S. Rosenzweig, V. Sulimov, Y. Takahashi, J. Wang

Florida State University, Tallahassee, Florida, USA
T. Adams, A. Al Kadhim, A. Askew, S. Bower, R. Goff, R. Hashmi, A. Hassani, R.S. Kim, T. Kolberg, G. Martinez, M. Mazza, H. Prosper, P.R. Prova, R. Yohay

Florida Institute of Technology, Melbourne, Florida, USA
B. Alsufyani, S. Butalla, S. Das, M. Hohlmann, M. Lavinsky, E. Yanes

University of Illinois Chicago, Chicago, Illinois, USA
M.R. Adams, N. Barnett, A. Baty, C. Bennett, R. Cavanaugh, R. Escobar Franco, O. Evdokimov, C.E. Gerber, H. Gupta, M. Hawksworth, A. Hingrajiya, D.J. Hofman, J.h. Lee, C. Mills, S. Nanda, G. Nigmatkulov, B. Ozek, T. Phan, D. Pilipovic, R. Pradhan, E. Prifti, P. Roy, T. Roy, N. Singh, M.B. Tonjes, N. Varelas, M.A. Wadud, J. Yoo

The University of Iowa, Iowa City, Iowa, USA
M. Alhusseini, D. Blend, K. Dilsiz[83], O.K. Köseyan, A. Mestvirishvili[84], O. Neogi,

H. Ogul[85], Y. Onel, A. Penzo, C. Snyder, E. Tiras[86]

Johns Hopkins University, Baltimore, Maryland, USA
B. Blumenfeld, J. Davis, A.V. Gritsan, L. Kang, S. Kyriacou, P. Maksimovic, M. Roguljic, S. Sekhar, M.V. Srivastav, M. Swartz

The University of Kansas, Lawrence, Kansas, USA
A. Abreu, L.F. Alcerro Alcerro, J. Anguiano, S. Arteaga Escatel, P. Baringer, A. Bean, R. Bhattacharya, Z. Flowers, D. Grove, J. King, G. Krintiras, M. Lazarovits, C. Le Mahieu, J. Marquez, M. Murray, M. Nickel, S. Popescu[87], C. Rogan, C. Royon, S. Rudrabhatla, S. Sanders, C. Smith, G. Wilson

Kansas State University, Manhattan, Kansas, USA
B. Allmond, N. Islam, A. Ivanov, K. Kaadze, Y. Maravin, J. Natoli, G.G. Reddy, D. Roy, G. Sorrentino

University of Maryland, College Park, Maryland, USA
A. Baden, A. Belloni, J. Bistany-riebman, S.C. Eno, N.J. Hadley, S. Jabeen, R.G. Kellogg, T. Koeth, B. Kronheim, S. Lascio, P. Major, A.C. Mignerey, C. Palmer, C. Papageorgakis, M.M. Paranjpe, E. Popova[88], A. Shevelev, L. Zhang

Massachusetts Institute of Technology, Cambridge, Massachusetts, USA
C. Baldenegro Barrera, H. Bossi, S. Bright-Thonney, I.A. Cali, Y.c. Chen, P.c. Chou, M. D'Alfonso, J. Eysermans, C. Freer, G. Gomez-Ceballos, M. Goncharov, G. Grosso, P. Harris, D. Hoang, G.M. Innocenti, K. Ivanov, D. Kovalskyi, J. Krupa, L. Lavezzo, Y.-J. Lee, K. Long, C. Mcginn, A. Novak, M.I. Park, C. Paus, C. Reissel, C. Roland, G. Roland, S. Rothman, T.a. Sheng, G.S.F. Stephans, D. Walter, Z. Wang, B. Wyslouch, T. J. Yang

University of Minnesota, Minneapolis, Minnesota, USA
B. Crossman, W.J. Jackson, C. Kapsiak, M. Krohn, D. Mahon, J. Mans, B. Marzocchi, R. Rusack, O. Sancar, R. Saradhy, N. Strobbe

University of Nebraska-Lincoln, Lincoln, Nebraska, USA
K. Bloom, D.R. Claes, G. Haza, J. Hossain, C. Joo, I. Kravchenko, A. Rohilla, J.E. Siado, W. Tabb, A. Vagnerini, A. Wightman, F. Yan

State University of New York at Buffalo, Buffalo, New York, USA
H. Bandyopadhyay, L. Hay, H.w. Hsia, I. Iashvili, A. Kalogeropoulos, A. Kharchilava, A. Mandal, M. Morris, D. Nguyen, S. Rappoccio, H. Rejeb Sfar, A. Williams, P. Young, D. Yu

Northeastern University, Boston, Massachusetts, USA
G. Alverson, E. Barberis, J. Bonilla, B. Bylsma, M. Campana, J. Dervan, Y. Haddad, Y. Han, I. Israr, A. Krishna, M. Lu, N. Manganelli, R. Mccarthy, D.M. Morse, T. Orimoto, L. Skinnari, C.S. Thoreson, E. Tsai, D. Wood

Northwestern University, Evanston, Illinois, USA
S. Dittmer, K.A. Hahn, M. Mcginnis, Y. Miao, D.G. Monk, M.H. Schmitt, A. Taliercio, M. Velasco, J. Wang

University of Notre Dame, Notre Dame, Indiana, USA
G. Agarwal, R. Band, R. Bucci, S. Castells, A. Das, A. Ehnis, R. Goldouzian, M. Hildreth, K. Hurtado Anampa, T. Ivanov, C. Jessop, A. Karneyeu, K. Lannon, J. Lawrence, N. Loukas, L. Lutton, J. Mariano, N. Marinelli, I. Mcalister,

T. McCauley, C. Mcgrady, C. Moore, Y. Musienko[22], H. Nelson, M. Osherson, A. Piccinelli, R. Ruchti, A. Townsend, Y. Wan, M. Wayne, H. Yockey

The Ohio State University, Columbus, Ohio, USA
A. Basnet, M. Carrigan, R. De Los Santos, L.S. Durkin, C. Hill, M. Joyce, M. Nunez Ornelas, D.A. Wenzl, B.L. Winer, B. R. Yates

Princeton University, Princeton, New Jersey, USA
H. Bouchamaoui, G. Dezoort, P. Elmer, A. Frankenthal, M. Galli, B. Greenberg, N. Haubrich, K. Kennedy, G. Kopp, Y. Lai, D. Lange, A. Loeliger, D. Marlow, I. Ojalvo, J. Olsen, F. Simpson, D. Stickland, C. Tully

University of Puerto Rico, Mayaguez, Puerto Rico, USA
S. Malik, R. Sharma

Purdue University, West Lafayette, Indiana, USA
S. Chandra, R. Chawla, A. Gu, L. Gutay, M. Jones, A.W. Jung, D. Kondratyev, M. Liu, G. Negro, N. Neumeister, G. Paspalaki, S. Piperov, N.R. Saha, J.F. Schulte, F. Wang, A. Wildridge, W. Xie, Y. Yao, Y. Zhong

Purdue University Northwest, Hammond, Indiana, USA
N. Parashar, A. Pathak, E. Shumka

Rice University, Houston, Texas, USA
D. Acosta, A. Agrawal, C. Arbour, T. Carnahan, P. Das, K.M. Ecklund, S. Freed, F.J.M. Geurts, T. Huang, I. Krommydas, N. Lewis, W. Li, J. Lin, O. Miguel Colin, B.P. Padley, R. Redjimi, J. Rotter, M. Wulansatiti, E. Yigitbasi, Y. Zhang

University of Rochester, Rochester, New York, USA
O. Bessidskaia Bylund, A. Bodek, P. de Barbaro[†], R. Demina, A. Garcia-Bellido, H.S. Hare, O. Hindrichs, N. Parmar, P. Parygin[88], H. Seo, R. Taus

Rutgers, The State University of New Jersey, Piscataway, New Jersey, USA
B. Chiarito, J.P. Chou, S.V. Clark, S. Donnelly, D. Gadkari, Y. Gershtein, E. Halkiadakis, C. Houghton, D. Jaroslawski, A. Kobert, S. Konstantinou, I. Laflotte, A. Lath, J. Martins, M. Perez Prada, B. Rand, J. Reichert, P. Saha, S. Salur, S. Schnetzer, S. Somalwar, R. Stone, S.A. Thayil, S. Thomas, J. Vora

University of Tennessee, Knoxville, Tennessee, USA
D. Ally, A.G. Delannoy, S. Fiorendi, J. Harris, T. Holmes, A.R. Kanuganti, N. Karunarathna, J. Lawless, L. Lee, E. Nibigira, B. Skipworth, S. Spanier

Texas A&M University, College Station, Texas, USA
D. Aebi, M. Ahmad, T. Akhter, K. Androsov, A. Bolshov, O. Bouhali[89], A. Cagnotta, V. D'Amante, R. Eusebi, P. Flanagan, J. Gilmore, Y. Guo, T. Kamon, S. Luo, R. Mueller, A. Safonov

Texas Tech University, Lubbock, Texas, USA
N. Akchurin, J. Damgov, Y. Feng, N. Gogate, Y. Kazhykarim, K. Lamichhane, S.W. Lee, C. Madrid, A. Mankel, T. Peltola, I. Volobouev

Vanderbilt University, Nashville, Tennessee, USA
E. Appelt, Y. Chen, S. Greene, A. Gurrola, W. Johns, R. Kunnawalkam Elayavalli, A. Melo, D. Rathjens, F. Romeo, P. Sheldon, S. Tuo, J. Velkovska, J. Viinikainen, J. Zhang

University of Virginia, Charlottesville, Virginia, USA
B. Cardwell, H. Chung, B. Cox, J. Hakala, G. Hamilton Ilha Machado, R. Hirosky, M. Jose, A. Ledovskoy, C. Mantilla, C. Neu, C. Ramón Álvarez, Z. Wu

Wayne State University, Detroit, Michigan, USA
S. Bhattacharya, P.E. Karchin

University of Wisconsin - Madison, Madison, Wisconsin, USA
A. Aravind, S. Banerjee, K. Black, T. Bose, E. Chavez, S. Dasu, P. Everaerts, C. Galloni, H. He, M. Herndon, A. Herve, C.K. Koraka, S. Lomte, R. Loveless, A. Mallampalli, A. Mohammadi, S. Mondal, T. Nelson, G. Parida, L. Pétré, D. Pinna, A. Savin, V. Shang, V. Sharma, W.H. Smith, D. Teague, H.F. Tsoi, W. Vetens, A. Warden

Authors affiliated with an international laboratory covered by a cooperation agreement with CERN
S. Afanasiev, V. Alexakhin, Yu. Andreev, T. Aushev, D. Budkouski, R. Chistov, M. Danilov, T. Dimova, A. Ershov, S. Gninenko, I. Gorbunov, A. Gribushin, A. Kamenev, V. Karjavine, M. Kirsanov, V. Klyukhin, O. Kodolova[90], V. Korenkov, I. Korsakov, A. Kozyrev, N. Krasnikov, A. Lanev, A. Malakhov, V. Matveev, A. Nikitenko[91,90], V. Palichik, V. Perelygin, S. Petrushanko, S. Polikarpov, O. Radchenko, M. Savina, V. Shalaev, S. Shmatov, S. Shulha, Y. Skovpen, K. Slizhevskiy, V. Smirnov, O. Teryaev, I. Tlisova, A. Toropin, N. Voytishin, A. Zarubin, I. Zhizhin

Authors affiliated with an institute formerly covered by a cooperation agreement with CERN
E. Boos, V. Bunichev, M. Dubinin[81], V. Savrin, A. Snigirev, L. Dudko, V. Kim[22], V. Murzin, V. Oreshkin, D. Sosnov

†: Deceased
[1]Also at Yerevan State University, Yerevan, Armenia
[2]Also at TU Wien, Vienna, Austria
[3]Also at Ghent University, Ghent, Belgium
[4]Also at Universidade do Estado do Rio de Janeiro, Rio de Janeiro, Brazil
[5]Also at FACAMP - Faculdades de Campinas, Sao Paulo, Brazil
[6]Also at Universidade Estadual de Campinas, Campinas, Brazil
[7]Also at Federal University of Rio Grande do Sul, Porto Alegre, Brazil
[8]Also at The University of the State of Amazonas, Manaus, Brazil
[9]Also at University of Chinese Academy of Sciences, Beijing
[10]Also at China Center of Advanced Science and Technology, Beijing
[11]Also at University of Chinese Academy of Sciences, Beijing
[12]Also at School of Physics, Zhengzhou University, Zhengzhou
[13]Now at Henan Normal University, Xinxiang
[14]Also at University of Shanghai for Science and Technology, Shanghai
[15]Now at The University of Iowa, Iowa City, Iowa, USA
[16]Also at Center for High Energy Physics, Peking University, Beijing
[17]Also at Helwan University, Cairo, Egypt
[18]Now at Zewail City of Science and Technology, Zewail, Egypt
[19]Also at British University in Egypt, Cairo, Egypt
[20]Also at Purdue University, West Lafayette, Indiana, USA
[21]Also at Université de Haute Alsace, Mulhouse, France
[22]Also at an institute formerly covered by a cooperation agreement with CERN

[23]Also at University of Hamburg, Hamburg, Germany
[24]Also at RWTH Aachen University, III. Physikalisches Institut A, Aachen, Germany
[25]Also at Bergische University Wuppertal (BUW), Wuppertal, Germany
[26]Also at Brandenburg University of Technology, Cottbus, Germany
[27]Also at Forschungszentrum Jülich, Juelich, Germany
[28]Also at CERN, European Organization for Nuclear Research, Geneva, Switzerland
[29]Also at HUN-REN ATOMKI - Institute of Nuclear Research, Debrecen, Hungary
[30]Now at Universitatea Babes-Bolyai - Facultatea de Fizica, Cluj-Napoca, Romania
[31]Also at MTA-ELTE Lendület CMS Particle and Nuclear Physics Group, Eötvös Loránd University, Budapest, Hungary
[32]Also at HUN-REN Wigner Research Centre for Physics, Budapest, Hungary
[33]Also at Physics Department, Faculty of Science, Assiut University, Assiut, Egypt
[34]Also at The University of Kansas, Lawrence, Kansas, USA
[35]Also at Punjab Agricultural University, Ludhiana, India
[36]Also at University of Hyderabad, Hyderabad, India
[37]Also at Indian Institute of Science (IISc), Bangalore, India
[38]Also at University of Visva-Bharati, Santiniketan, India
[39]Also at IIT Bhubaneswar, Bhubaneswar, India
[40]Also at Institute of Physics, Bhubaneswar, India
[41]Also at Deutsches Elektronen-Synchrotron, Hamburg, Germany
[42]Also at Isfahan University of Technology, Isfahan, Iran
[43]Also at Sharif University of Technology, Tehran, Iran
[44]Also at Department of Physics, University of Science and Technology of Mazandaran, Behshahr, Iran
[45]Also at Department of Physics, Faculty of Science, Arak University, ARAK, Iran
[46]Also at Centro Siciliano di Fisica Nucleare e di Struttura Della Materia, Catania, Italy
[47]Also at Università degli Studi Guglielmo Marconi, Roma, Italy
[48]Also at Scuola Superiore Meridionale, Università di Napoli 'Federico II', Napoli, Italy
[49]Also at Fermi National Accelerator Laboratory, Batavia, Illinois, USA
[50]Also at Lulea University of Technology, Lulea, Sweden
[51]Also at Consiglio Nazionale delle Ricerche - Istituto Officina dei Materiali, Perugia, Italy
[52]Also at UPES - University of Petroleum and Energy Studies, Dehradun, India
[53]Also at Institut de Physique des 2 Infinis de Lyon (IP2I), Villeurbanne, France
[54]Also at Department of Applied Physics, Faculty of Science and Technology, Universiti Kebangsaan Malaysia, Bangi, Malaysia
[55]Also at Trincomalee Campus, Eastern University, Sri Lanka, Nilaveli, Sri Lanka
[56]Also at Saegis Campus, Nugegoda, Sri Lanka
[57]Also at National and Kapodistrian University of Athens, Athens, Greece
[58]Also at Ecole Polytechnique Fédérale Lausanne, Lausanne, Switzerland
[59]Also at Universität Zürich, Zurich, Switzerland
[60]Also at Stefan Meyer Institute for Subatomic Physics, Vienna, Austria
[61]Also at Near East University, Research Center of Experimental Health Science, Mersin, Turkey
[62]Also at Konya Technical University, Konya, Turkey
[63]Also at Izmir Bakircay University, Izmir, Turkey
[64]Also at Adiyaman University, Adiyaman, Turkey
[65]Also at Bozok Universitetesi Rektörlügü, Yozgat, Turkey
[66]Also at Istanbul Sabahattin Zaim University, Istanbul, Turkey
[67]Also at Marmara University, Istanbul, Turkey

[68]Also at Milli Savunma University, Istanbul, Turkey
[69]Also at Informatics and Information Security Research Center, Gebze/Kocaeli, Turkey
[70]Also at Kafkas University, Kars, Turkey
[71]Now at Istanbul Okan University, Istanbul, Turkey
[72]Also at Istanbul University - Cerrahpasa, Faculty of Engineering, Istanbul, Turkey
[73]Also at Istinye University, Istanbul, Turkey
[74]Also at Yildiz Technical University, Istanbul, Turkey
[75]Also at School of Physics and Astronomy, University of Southampton, Southampton, United Kingdom
[76]Also at Monash University, Faculty of Science, Clayton, Australia
[77]Also at Bethel University, St. Paul, Minnesota, USA
[78]Also at Università di Torino, Torino, Italy
[79]Also at Karamanoğlu Mehmetbey University, Karaman, Turkey
[80]Also at California Lutheran University;, Thousand Oaks, California, USA
[81]Also at California Institute of Technology, Pasadena, California, USA
[82]Also at United States Naval Academy, Annapolis, Maryland, USA
[83]Also at Bingol University, Bingol, Turkey
[84]Also at Georgian Technical University, Tbilisi, Georgia
[85]Also at Sinop University, Sinop, Turkey
[86]Also at Erciyes University, Kayseri, Turkey
[87]Also at Horia Hulubei National Institute of Physics and Nuclear Engineering (IFIN-HH), Bucharest, Romania
[88]Now at another institute formerly covered by a cooperation agreement with CERN
[89]Also at Hamad Bin Khalifa University (HBKU), Doha, Qatar
[90]Also at Yerevan Physics Institute, Yerevan, Armenia
[91]Also at Imperial College, London, United Kingdom